Satellite Detection of NO$_2$ Distributions Using TROPOMI and TEMPO and Comparison with Ground-Based Concentrations

Summer Acker,[1] Tracey Holloway[1,2] and Monica Harkey[1]

[1] Nelson Institute Center for Sustainability and the Global Environment, University of Wisconsin-Madison, Madison, WI 53705, United States of America

[2] Department of Atmospheric and Oceanic Sciences, University of Wisconsin-Madison, Madison, WI 53705, United States of America

Correspondence to: Tracey Holloway (taholloway@wisc.edu)

Abstract

In this study we assess the capability of current-generation satellites to capture the variability of near-surface nitrogen dioxide (NO$_2$) monitoring data, with the goal of supporting health and regulatory applications. We consider NO$_2$ vertical column densities (VCD) over the United States from two satellite instruments, the Tropospheric Monitoring Instrument (TROPOMI), and Tropospheric Emissions: Monitoring of Pollution (TEMPO), and compare with ground-based concentrations as measured by the EPA's Air Quality System (AQS) monitors. While TROPOMI provides a longer-term record of assessment (2019-2023), TEMPO informs diurnal patterns relevant to evaluating peak NO$_2$. We analyze frequency distributions and quantify their similarity using the Jensen-Shannon Divergence (JSD), where smaller values indicate better agreement. Satellite and ground monitor NO$_2$ distributions are most similar at non-roadway monitors (JSD = 0.008) and are most different at interstate (JSD = 0.158) and highway (JSD = 0.095) monitors. Seasonal analysis shows the most similarity in distributions in winter (JSD = 0.010), and the most difference in summer (JSD = 0.035). Across seasons and monitor locations, the calculated 1:30 pm LT TEMPO consistently exhibits better or comparable JSDs to TROPOMI (TEMPO: 0.005 to 0.151; TROPOMI: 0.012 to 0.265). TEMPO's agreement with monitors in both December 2023 and July 2024 is found to be best around midday, with non-road monitors in July having the best alignment (JSD = 0.008) at 16 UTC (~11 am LT). These

30 findings highlight the ability of TROPOMI and TEMPO to complement existing ground-based

31 monitors, and demonstrate their potential for monitor siting, regulatory, and public health

32 applications.

1 Introduction

34 Nitrogen dioxide (NO_2) is a gas released through high temperature combustion processes such as

35 the burning of fossil fuels (Lee et al., 1997; Richter et al., 2005), with on-road vehicles, power

36 plants, and industrial processes representing the largest anthropogenic sources in the United

37 States (U.S.; van der A et al., 2008) as well as lightning NO_X emissions (Dang et al., 2023) and

38 soil microbial activity (Huber et al., 2020) from natural sources. Exposure to elevated levels of

39 NO_2 has been linked to respiratory and cardiovascular diseases (Mills et al., 2015; Urbanowicz et

40 al., 2023; Meng et al., 2021), especially asthma in children (Mölter et al., 2014; Anenberg et al.,

41 2022; Achakulwisut et al., 2019), as well as premature mortality (Camilleri et al., 2023; Hales et

42 al., 2021; Huangfu and Atkinson, 2020), and other diseases (Xia et al., 2024; Bai et al., 2018).

43 NO_2 plays a critical role in the formation of ozone, which also causes respiratory health problems

44 and is harmful to ecosystems (Grulke & Heath, 2019; Sillman, 1999). It is also a precursor to

45 nitrate (Behera & Sharma, 2012), a type of fine particulate matter ($PM_{2.5}$), which can penetrate

46 deep into the lungs and exacerbate respiratory and heart conditions (Sangkham et al., 2024;

47 Sharma et al., 2020), as well as cause premature death (Orellano et al., 2020; Thangavel et al.,

48 2022).

49 Due to its radiative characteristics, NO_2 may be observed by satellites during daylight hours

50 (Boersma et al., 2018; Van Geffen et al., 2020; Veefkind et al., 2012), and NO_2 has emerged as

51 one of the most air-quality-relevant pollutants from satellites (Holloway et al., 2021). Several

52 studies have highlighted the potential for satellite NO_2 data to supplement ground-based

53 networks to support health analysis and air quality management (Duncan et al., 2014; Lee &

54 Koutrakis, 2014). The 2017 launch of the Tropospheric Monitoring Instrument (TROPOMI;

55 Boersma et al., 2018; Van Geffen et al., 2020; Veefkind et al., 2012) advanced these applications

56 (Goldberg et al., 2021; Griffin et al., 2019; Kim et al., 2024; Yu & Li, 2022; Dressel et al., 2022;

57 Goldberg et al., 2024; H. J. Lee et al., 2023). The Tropospheric Emissions: Monitoring of

58 Pollution (TEMPO; Chance et al., 2019; Naeger et al., 2021; Zoogman et al., 2017) provides

59 further advancements with daytime hourly observations of NO_2 over North America and finer

60 spatial coverage.

61 While advanced methods exist to calculate near-surface NO_2 from satellite columns (Ahmad et

62 al., 2024; Kim et al., 2021; Shetty et al., 2024; Virta et al., 2023), there is also a strong interest in

63 the utilization of satellite vertical column density (VCD) to directly infer NO_2 concentrations

64 analogous to ground-based monitors (Kim et al., 2024; Lamsal et al., 2014; Griffin et al., 2019;

65 Yu & Li, 2022; Zhang et al., 2018; Lamsal et al., 2015; Goldberg et al., 2021; Dressel et al.,

66 2022; Goldberg et al., 2024; Harkey & Holloway, 2024; Bechle et al., 2013; H. J. Lee et al.,

67 2023; Xu & Xiang, 2023). This study extends prior assessments of NO_2 column-to-surface

68 agreement, where we focus on frequency distributions to capture the net impact of day-to-day

69 variability.

70 The relationship between surface NO_2 and column abundance is influenced by physical and

71 chemical processes, many of which have seasonal components. In winter, shallow boundary

72 layers trap pollutants near the surface, leading to higher surface concentrations and increasing

73 surface-to-column agreement (Harkey et al., 2015). In summer, higher temperatures and

74 increased sunlight accelerate photochemical reactions, converting NO_2 into ozone and other

75 secondary pollutants, and decreasing surface-to-column agreement (Boersma et al., 2009).

76 Seasonal changes in emissions, such as high building-heating emissions in winter, and high

77 power plant emissions in summer (Frost et al., 2006; Levinson & Akbari, 2010) interact with

78 atmospheric processes causing an increase in NO_2 column abundance in winter in four-season

79 climates (Shah et al., 2020). Processes affecting the sources and sinks of NO_2 at the surface and

80 through the vertical column can also lead to temporal lags, with peak surface NO_2 preceding

81 peak column NO_2 in the mornings (Harkey et al. 2024).

82 Frequency distributions capture the variability, extremes, and patterns of pollutant abundance,

83 relevant to air quality standards, pollution trends, and the effectiveness of emission control

84 measures (Knox and Lange, 1974; Pollack, 1975; Venkatram, 1979; Chowdhury et al., 2021;

85 Mondal et al., 2021). For example, Mondal et al. (2021) used frequency distributions of ground-

86 based monitors to examine changes in air quality across Delhi and Kolkata during COVID-19

87 lockdown phases, showing how reduced human activity led to shifts in pollutant levels. We

88   extend this line of analysis by comparing NO_2 distributions across multiple dimensions with

89   TROPOMI and include time-of-day and resolution-dependence of results using data from

90   TEMPO.

91   In this work, we consider: (1) How do the distributions of satellite NO_2 VCD compare with those

92   for near-surface NO_2? (2) To what degree does new hourly data from TEMPO improve the

93   agreement between surface and space based NO_2 distributions? For both questions, we consider

94   spatial variability, especially proximity to roadways, and temporal variability including

95   seasonality and diurnal variability. By considering the ability of satellites to capture peak NO_2

96   values in a comparable distribution to surface data, we consider how satellite VCDs can support

97   air quality management, improve health impact analysis, and inform air pollution monitor siting.

98   **2 Data and Methods**

99   In this study, we evaluate the ability of two satellite instruments, TROPOMI and TEMPO, to

100   capture the spatial and temporal variability in NO_2 surface concentration distributions across the

101   continental United States (CONUS), as measured by AQS monitors. By comparing the

102   coefficient of variation (CV) and Jensen-Shannon divergence (JSD) between satellite and

103   monitor data, we aim to assess the alignment between the datasets.

104   **2.1 EPA Surface Monitor Data**

105   The Environmental Protection Agency (EPA) Air Quality System (AQS) contains hourly NO_2

106   measurements from ground-based monitors, providing high temporal resolution data that are

107   critical for assessing compliance with the U.S. National Ambient Air Quality Standards

108   (NAAQS). There are two NAAQS related to NO_2: one for annual average concentration, set at

109   53 ppb, and one based on peak 1-hour concentrations, set at 100 ppb, based on the 3-year

110   average of the 98th percentile of the yearly distribution of 1-hour daily maximum NO_2

111   concentrations (EPA, 2010). Enforcement of these standards relies on data from AQS NO_2

112   monitors, a network that includes 431 monitors as of August 2024. Because NO_2 has a relatively

113   short atmospheric lifetime, typically ranging from a few hours to a day depending on

114   meteorological conditions (Lange et al., 2022; Liu et al., 2021), ground monitors are expected to

115   capture local conditions (Wang et al., 2020).

The EPA AQS data (EPA, 2025) was used to access NO_2 monitor data for the years 2019 through 2023 from all available sites in CONUS during this time period (503 unique monitors from 2019 to 2023). We note that there are some areas that are overrepresented by NO_2 monitors, and others that are lacking monitors. Specifically, most monitors are located in urban areas, especially on the East Coast and in Southern California, meaning that rural areas tend to be less represented by ground monitors (Kerr et al., 2023). Most monitors use a chemiluminescence method, where the amount of NO_2 that is converted to NO is measured by a molybdenum oxide converter (Fontijn et al., 1970). The converter also reacts with other oxidized nitrogen compounds such as nitric acid (HNO_3) and peroxyacetyl nitrate (PAN) to form NO (Dunlea et al., 2007; Steinbacher et al., 2007), which can lead to an overestimation of NO_2. Corrections for this bias have been applied when comparing with satellite observations (e.g. Cooper et al., 2020; Lamsal et al., 2015; Li et al., 2021). Uncorrected AQS NO_2 has been used for determining compliance with the NAAQS and for health assessments, which is the approach we take here, consistent with prior studies focused on regulatory relevance (Novotny et al., 2011; Penn & Holloway, 2020; Harkey and Holloway, 2024; Goldberg et al., 2021; Kim et al., 2024; Duncan et al., 2013; Qin et al., 2019). More recently, some NO_2 monitors have been added to the network which measure "true NO_2" using Cavity Attenuated Phase Shift Spectroscopy (CAPS, Kebabian et al., 2005). These monitors are expected to be more representative of ground-level NO_2 concentrations and should have less overestimations since they directly measure NO_2 and no other species (Ge et al., 2013). Some of the monitors used in this study use CAPS methodology to measure NO_2. We discuss the comparison of CAPS versus traditional NO_2 monitors in results Sect. 3.1.

Hourly AQS measurements at 13:00 and 14:00 local time (LT) were averaged to align with the TROPOMI overpass of ~13:30 LST. Hourly AQS measurements from 12:00 GMT to 23:00 GMT are compared with hourly TEMPO data for daylight hours. For both the TROPOMI and TEMPO analyses, AQS data are filtered to ensure consistency with satellite data availability. As a result of filtering monitoring data for TROPOMI and TEMPO separately, the subsets of monitor data available for comparison with each instrument differ, even for the same time periods.

2.2 TROPOMI Data

145 The Tropospheric Monitoring Instrument (TROPOMI; European Space Agency, 2021) is on

146 board the Copernicus Sentinel-5 Precursor satellite which has a daily, local overpass time of

147 ~13:30 LST (Veefkind et al., 2012). Currently, the highest resolution of TROPOMI is 3.5 km by

148 5.5 km at nadir which has increased from 3.5 km by 7.0 km since August 6th, 2019. Daily

149 TROPOMI NO_2 data for the years 2019 through 2023 were allocated to a 4 km x 4 km grid over

150 CONUS using the Wisconsin Horizontal Interpolation Program for Satellites (WHIPS; Center

151 for Sustainability and the Global Environment, 2024; Harkey et al., 2015, 2021; Harkey and

152 Holloway, 2024; Penn and Holloway, 2020). Using WHIPS, we also remove data with a quality

153 flag lower than 0.75. Each monitor location was compared with the 4 km x 4 km gridded

154 TROPOMI value in the corresponding grid cell. December 2023 and July 2024 4 km x 4 km

155 TROPOMI NO_2 data were also collected for each of the monitors for comparison with TEMPO

156 data.

157 A 4 km x 4 km oversampled grid is used as opposed to the 1 km x 1 km oversampled grid since

158 this study focuses on daily observations, and the 1 km x 1 km grid is best suited for monthly or

159 annual averages (Goldberg et al., 2021). To ensure a valid number of TROPOMI pixels were

160 being represented despite the higher grid resolution, we analyzed the number of ground monitors

161 falling within each TROPOMI pixel by performing a spatial join between ground monitor

162 locations and the oversampled 4 km x 4 km TROPOMI grid. About 97% of TROPOMI pixels

163 contain only one monitor, with only a small number of pixels (2.7%) containing more than one.

164 Figure S1 shows the number of monitors per TROPOMI pixel (locations where there are more

165 than 1 monitor per TROPOMI pixel) and the number of valid TROPOMI retrievals from 2019 to

166 2023 at each grid cell, confirming that monitors are well-distributed enough to not

167 disproportionately cluster within a small subset of satellite pixels. Since monitors are spread

168 across the entire U.S. and most are at least 4 km apart, there is generally sufficient separation to

169 ensure that most monitors are assigned to distinct TROPOMI pixels rather than falling into the

170 same grid cells repeatedly.

171 **2.3 TEMPO Data**

172 The TEMPO instrument launched onboard the Intelsat 40e mission (NASA, 2024), a

173 geostationary satellite, on April 7, 2023. TEMPO provides hourly measurements of atmospheric

174 pollutants over North America (Chance et al., 2019; Naeger et al., 2021; Zoogman et al., 2017).

175 TEMPO achieves a spatial resolution of approximately 2.1 km in the north-south direction and

176 4.5 km in the east-west direction at the center of its Field of Regard (FOR), centered around

177 36.5° N and 100° W (Chance et al., 2019). The TEMPO Level-3 (L3) NO_2 data (Suleiman, 2024)

178 used in this study were accessed through NASA's EarthData Search portal.

179 In order to synchronize TEMPO and ground-based hourly measurements, TEMPO timestamps

180 were rounded to the nearest hour, with mid-hour values rounded up. All files within each

181 rounded-hour group were averaged, producing a single NO_2 value per hour per day. Only

182 TEMPO observations with a main data quality flag of 0 and cloud fraction at or less than 0.2

183 were retained, in line with TEMPO documentation guidelines (NASA Langley Research Center,

184 2024).

185 For the comparison with TROPOMI, the UTC equivalents of 1 pm and 2 pm LT were

186 determined for each time zone based on the latitude and longitude of each monitor location.

187 TEMPO NO_2 values corresponding to these calculated UTC hours were averaged to align with

188 the TROPOMI overpass time (~13:30 LST). Similarly, for ground-based measurements, the

189 monitor data were filtered to include only values corresponding to 1 pm and 2 pm LT and then

190 averaged.

191 **2.4 Monitor Classification**

192 To classify the monitors by roadway proximity, the state-level Census Bureau's 2021

193 TIGER/Line shapefiles for Primary and Secondary Roads (2021 TIGER/Line® Shapefiles,

194 2025) were combined to form a comprehensive dataset for the CONUS domain.

195 To evaluate how TROPOMI and ground-based monitor NO_2 values vary by proximity to a road,

196 monitors were also assigned to different groups based on their distance from a road (≤20-m, 20

197 to 50-m, 50 to 300-m, 300-m to 1 km, and > 1 km), where buffer distances are calculated from

198 the road shapefiles (Figure S3). There were 9 monitors that were 20 meters or less away from a

199 road, 66 between 20 and 50 meters from a road, 108 between 50 and 300 meters, 167 between

200 300 meters and 1 kilometer, and 153 that were greater than 1 kilometer from a road.

201 Roads were also classified into three categories: (1) interstates, (2) highways, and (3) other

202 roads, based on their route type code (RTTYP) values. Where monitors are considered as

203 representing a roadway category, we followed the criteria of the EPA Near-Road-Network

204 (Gantt et al., 2021; Kim et al., 2024) to merge monitor locations with road buffers, considering

205 the 50-m buffer recommended by the EPA, as well as a less restrictive 300-m buffer. In each

206 case, monitors inside the buffer of a particular roadway type were classified as representing that

207 category. If a monitor fell within multiple buffers, it was assigned the classification of the largest

208 road type. Monitors not falling within any buffers were classified as "non-roadway."

209 Using the 50-m buffer, 58 monitors were classified as "interstate," 17 as "highway," and 428 as

210 "non-roadway" (Figure S2; no monitors classified as "other roads"). Using the 300-m buffer, 91

211 monitors were classified as "interstate," 90 as "highway," 320 as "non-roadway," and 2 as "other

212 roads." Since there were no monitors classified as "other roads" for the 50-m buffer, this

213 category is excluded from the analysis.

214 We classified interstate monitors as urban or rural using the U.S. Census Bureau 2020 Urban

215 Areas Tiger/Line Shapefile (U.S. 2020 Urban Areas Shapefile, 2025). Only one interstate

216 monitor was identified as rural, so this analysis is not included.

217 **2.5 Data Analysis**

218 The coefficient of variation (CV) was calculated for ground-level monitor data and for satellite

219 data. This metric was used to compare the relative variability of NO_2 between satellite and

220 ground-level data despite different measurement units (Aerts et al., 2015). CV is defined as the

221 ratio of the standard deviation (σ) to the mean (μ) of the data:

222 $$CV = \left(\frac{\sigma}{\mu}\right) \times 100$$

223 The Jensen-Shannon Divergence (JSD) is used to quantify the similarity between the

224 distributions of NO_2 from the satellite and ground-level monitors despite the different

225 measurement units (Menéndez et al., 1997). The JSD is a robust metric for comparing

226 probability distributions that is used within a wide variety of fields, including machine learning

227 (Thiagarajan & Ghosh, 2024; Saurette et al., 2023; Tsigalou et al., 2021; Melville et al., 2005),

228 data science (Toledo et al., 2022; Zhao et al., 2024), biology (Yan et al., 2021; Jones et al., 2023;

229 Ahmed et al., 2023), and meteorology (Kibirige et al., 2023). In environmental research using

230 satellite data, the JSD has shown that the Mangrove Forest Index (MFI) from Sentinel-2 imagery

231 outperforms traditional vegetation indices in distinguishing submerged mangrove forests (Jia et

232 al., 2019). In air quality, the JSD has been used to compare modeled and measured $PM_{2.5}$ (Yang

233 et al., 2024), and to compare an air quality index (AQI) with measurements of specific air

234 pollutants (Wang & Zhang, 2022).

235 To calculate the JSD, each dataset was binned, with a bin size of 1 ppb (for ground monitors) or

236 1×10^{15} molecules/cm^2 (for satellite data), ranging from 0 to 40 ppb or 40×10^{15} molecule/cm^2,

237 with an additional bin for values exceeding 40 ppb or 40×10^{15} molecule/cm^2. For visualization

238 purposes, the frequency distributions are binned with the ground monitors ranging from 0 to 40

239 ppb and the satellite data ranging from 0 to 30×10^{15} molecule/cm^2, with an additional bin for

240 values exceeding 40 ppb or 30×10^{15} molecule/cm^2. Depending on the specific analysis, NO_2

241 data are grouped by: (1) Distance from roadways (in meters) – TROPOMI daily data from 2019

242 to 2023 (and corresponding ground monitors) are grouped by proximity to roads to assess spatial

243 alignment; (2) season – TROPOMI daily data from 2019 to 2023 (and corresponding ground

244 monitors) are grouped by season to analyze temporal alignment; (3) month – TROPOMI daily

245 data from December 2023 and July 2024, along with TEMPO and ground monitors at the

246 TROPOMI overpass time (~1:30 pm LT, represented by the average of 1 pm and 2 pm LT data),

247 are grouped by month to compare the temporal differences in alignment between TEMPO and

248 TROPOMI; and (4) road type (interstate, highway, non-roadway) – Both TROPOMI (daily),

249 TEMPO (calculated overpass time and hourly), and ground monitor data are grouped by road

250 type to evaluate varying alignment based on road classifications.

251 Binned data were then normalized to form probability distributions. The divergence was

252 calculated as:

$$JSD(P, Q) = \frac{1}{2} [D_{KL}(P||M) + D_{KL}(Q||M)]$$

253

254   where P and Q represent the probability distributions from the monitor and satellite data,

255   respectively, and M is the average of P and Q. The divergence D_{KL} is the Kullback-Leibler

256   divergence between each distribution and their mean (Clim et al., 2018). JSD values range from

257   0 to 1, with lower values indicating greater similarity between the satellite and monitor

258   distributions. In general, a JSD < 0.1 indicates very good alignment, $0.1 \leq$ JSD < 0.3 indicates

259   moderate alignment, and JSD $\geq$ 0.3 (Kibirige et al., 2023) indicates poor alignment.

260   **3 Results**

261   To evaluate the agreement between satellite and monitored NO_2 distributions, we consider the

262   impact of monitor location using TROPOMI; impact of season using TROPOMI; the comparison

263   of distributions between TROPOMI and TEMPO; and the impact of time-of-day using TEMPO.

264   **3.1 Alignment of TROPOMI NO_2 Distributions with Surface NO_2 Distributions**

265   This section analyzes TROPOMI and ground-based NO_2 measurements across varying distances

266   from roads, different seasons, and at monitors located near interstates, highways, and non-

267   roadway sites. Our results show that as the distance from roads increases, the distributions of

268   surface and column NO_2 become more similar. Monitor distributions near interstates and

269   highways exhibit lower agreement with TROPOMI distributions compared to those farther from

270   major roadways. Seasonally, alignment is strongest in winter and weakest in summer.

271   Figure 1 illustrates the distribution of NO_2 levels measured by AQS ground-based monitors and

272   TROPOMI observations as a function of distance from roadways using daily measurements from

273   2019 to 2023. For both data sources, mean, peak, and minimum NO_2 are all highest in the 20 –

274   50 m distance category (the second closest near-road category). NO_2 abundance decreases as

275   distance-to-road increases, and to a lesser extent as distance-to-road decreases. The somewhat

276   lower abundance in the $\leq$ 20 m category vs. the 20 – 50 m category may be due to the speciation

277   of NO_X, where nitric oxide (NO) is more abundant and converts to a higher fraction of NO_2 as

278   distance-to-road increases (Kimbrough et al., 2017). Most direct vehicle emissions are in the

279   form of NO, and close to the roadway, NO and NO_2 readily convert between forms. Limited

280   ozone availability—especially during stable conditions, which contribute to suppressed vertical

281   mixing—can slow the conversion of NO to NO_2 (Richmond-Bryant et al., 2017). As a result,

282   NO_2 may initially be suppressed very close to the road, and changes in total NO_X are primarily

283 driven by mixing and dilution rather than chemical transformation. NO_2 peaks in the 20–50 m

284 range likely because this zone allows for sufficient time and space for NO to oxidize to NO_2

285 while still being close enough to the emission source to experience elevated concentrations;

286 beyond this range, concentrations decrease with distance due to dispersion and dilution of

287 pollutants into the surrounding atmosphere. Mean monitored NO_2 is 6.85 ppb at $\leq$ 20 m, 10.47

288 ppb at 20 – 50 m, 4.53 ppb at 50 – 300 m, 3.71 ppb at 300 m – 1 km, and 2.80 ppb at > 1 km.

289 Mean TROPOMI NO_2 is 3.38 x 10^{15} molecules/cm^2 at $\leq$ 20 m, 4.21 10^{15} molecules/cm^2 at 20 –

290 50 m, 3.00 x 10^{15} molecules/cm^2 at 50 – 300 m, 3.72 x 10^{15} molecules/cm^2 at 300 m – 1 km, and

291 3.13 x 10^{15} molecules/cm^2 at > 1 km. Monitor values show a higher sensitivity to roadway

292 proximity, where the highest mean monitored concentration is 375% of the lowest mean

293 concentration, compared to TROPOMI where the highest mean VCD is 140% of the lowest

294 mean VCD.

295 Monitored NO_2 levels drop over 50% at ~50 m from the roadway (based on change in the mean,

296 upper 2.5 interquartile range, IQR, and the upper 1.5 IQR), a finding that compares with a 31%

297 reduction in NO_2 between 20m and 300m from Kimbrough et al. (2017), as well as other studies

298 that identify a decrease in NO_2 at further distances (Karner et al., 2010; Richmond-Bryant et al.,

299 2017). TROPOMI VCDs also show the greatest change with roadway distance at ~50 km, but by

300 less than 30% (based on change in the mean, upper 2.5 IQR, and the upper 1.5 IQR).

301 Just as total NO_2 abundance, from both monitors and satellite, is highest at distances of 20-50 m

302 from the roadway, the range of daily values is also widest for the 20 – 50 m range and smallest at

303 the > 1 km range. Monitored values have a standard deviation of 8.24 ppb in the 20 – 50 m

304 range, and a standard deviation of 3.39 ppb in the > 1 km range. The distribution of satellite data

305 does not vary as much in size across roadway locations, with a standard deviation of 3.90 x 10^{15}

306 molecules/cm^2 for the 20 – 50 m range and 3.31 x 10^{15} molecules/cm^2 for the > 1 km range. In

307 the 20 – 50 m range, the upper IQR of AQS NO_2 is 38% higher than the mean. TROPOMI shows

308 less variability than the monitors, with the 20 – 50 m upper IQR 16% higher than the mean. As

309 distance from the roadway increases, the distributions of data from the ground and satellite

310 become more comparable. In the > 1 km range, the upper IQR of monitor NO_2 is 23% higher

311 than the mean and the upper IQR of satellite data is 15% higher than the mean. The ranges show

312 more similarity at greater distances from the roadway, but even at distances of > 1 km, the range

313 of monitored values exceeds the range of satellite VCDs. These patterns agree with Kim et al.

314 (2024), who found that surface monitors show better agreement with TROPOMI further from

315 major roads. This improved alignment at greater distances likely reflects the reduced influence of

316 localized emission sources, which tend to create sharp gradients and rapid variability near roads.

317 In areas further from traffic, NO_2 concentrations vary more gradually or are generally more

318 uniform. As a result, surface monitors away from roads reflect broader conditions, in better

319 agreement with the coarser spatial resolution of TROPOMI.

320 When analyzed by season (Figure S4), the relationships are similar, except winter shows the

321 highest IQRs, with the 20 to 50 m distance group having an IQR of 11.40 ppb for monitors and

322 4.96 x 10^{15} molecules/cm^2 for TROPOMI, and summer, the lowest IQRs for both monitors (IQR

323 = 9.05 ppb) and TROPOMI (IQR = 1.71 x 10^{15} molecules/cm^2). In the greater than 1 km distance

324 group, again winter has the highest IQRs (monitor IQR = 4.60 ppb; TROPOMI IQR = 3.95 x

325 10^{15} molecules/cm^2) and summer the lowest IQRs (monitor IQR = 2.05 ppb; TROPOMI IQR =

326 1.55 x 10^{15} molecules/cm^2).

327

328
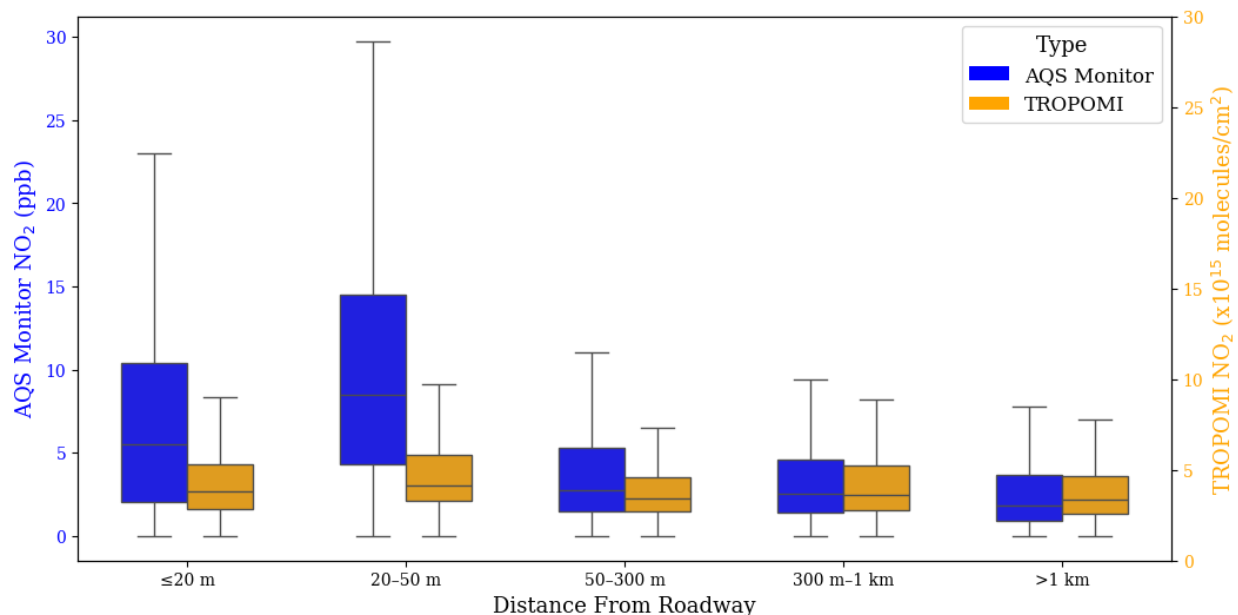
329 Figure 1. Box plots show median and interquartile ranges of all daily 2019 to 2023 NO_2 as

330 measured by AQS monitors (blue) and TROPOMI (orange) across various distances from

331 roadways, with the whiskers extending to the 1.5 IQR range. No outliers are shown. The left y-

332   axis represents AQS monitor values in parts per billion (ppb), and the right y-axis represents

333   TROPOMI NO_2 values in 10^{15} molecules per cm^2. The distance categories from the roadway

334   include $\leq$ 20 m, 20-50 m, 50-300 m, 300 m-1 km, and > 1 km.

335   To consider the shape of monitored and satellite NO_2 distributions, we consider the effect of

336   season in Fig. 2. The winter distributions (Figure 2a, calculated from December, January, and

337   February data) exhibit the longest tails and highest NO_2 values. In winter, the 90th percentile of

338   monitoring data is 14.80 ppb and the 90th percentile of TROPOMI data is 10.93 x 10^{15}

339   molecules/cm^2. Spring distributions (Figure 2b; March, April, and May) show intermediate

340   behavior, with lower values and shorter tails than winter and fall, but higher than summer (90th

341   percentile from monitors = 9.71 ppb; 90th percentile from TROPOMI = 6.19 x 10^{15}

342   molecules/cm^2). In summer (Figure 2c, June, July, and August), the distributions exhibit the

343   shortest tails, and the lowest NO_2 values (90th percentile from monitors = 9.00 ppb; 90th

344   percentile from TROPOMI = 4.57 x 10^{15} molecules/cm^2). Fall (Figure 2d; September, October,

345   and November) also shows intermediate behavior, generally between winter and spring (90th

346   percentile from monitors = 12.15 ppb; 90th percentile from TROPOMI = 7.44 x 10^{15}

347   molecules/cm^2). The higher NO_2 values in winter from monitor and TROPOMI data are

348   attributed to reduced photochemical activity in winter leading to longer NO_2 lifetimes (Harkey et

349   al., 2015; Boersma et al., 2009; Shah et al., 2020).

350   The highest percent frequencies for the monitor and TROPOMI distributions generally occur

351   within the 1–2 ppb or 1–2 x 10^{15} molecules/cm^2 bin. However, the winter TROPOMI distribution

352   peaks in the 2–3 x 10^{15} molecules/cm^2 bin with a percent frequency of 18.14%, compared with

353   winter monitor highest frequency of 14.33%. The highest percent frequency in spring from

354   TROPOMI is 30.39% versus monitor 24.15%; in summer TROPOMI is 34.35% versus monitor

355   of 24.68%; in fall TROPOMI is 24.90% versus monitor of 18.89%. These results indicate that

356   TROPOMI consistently records higher peak frequencies than the monitors, whereas monitors

357   consistently show a wider distribution.

358   Figure 2 provides a seasonal breakdown of the coefficient of variation (CV) and Jensen-Shannon

359   divergence (JSD) for both monitor and TROPOMI data across all monitors. Summer exhibits the

360   highest variability in monitored NO_2 concentrations (CV = 127.99%), but the lowest variability

361   in satellite observations (CV = 78.00%). The highest variability in TROPOMI occurs in winter

362   (CV = 103.51%), similar to the variability from monitor data (CV = 104.48%). Satellite CVs

363   generally follow a similar pattern to that of monitors, though the overall variability is lower for

364   satellite data across seasons.

365
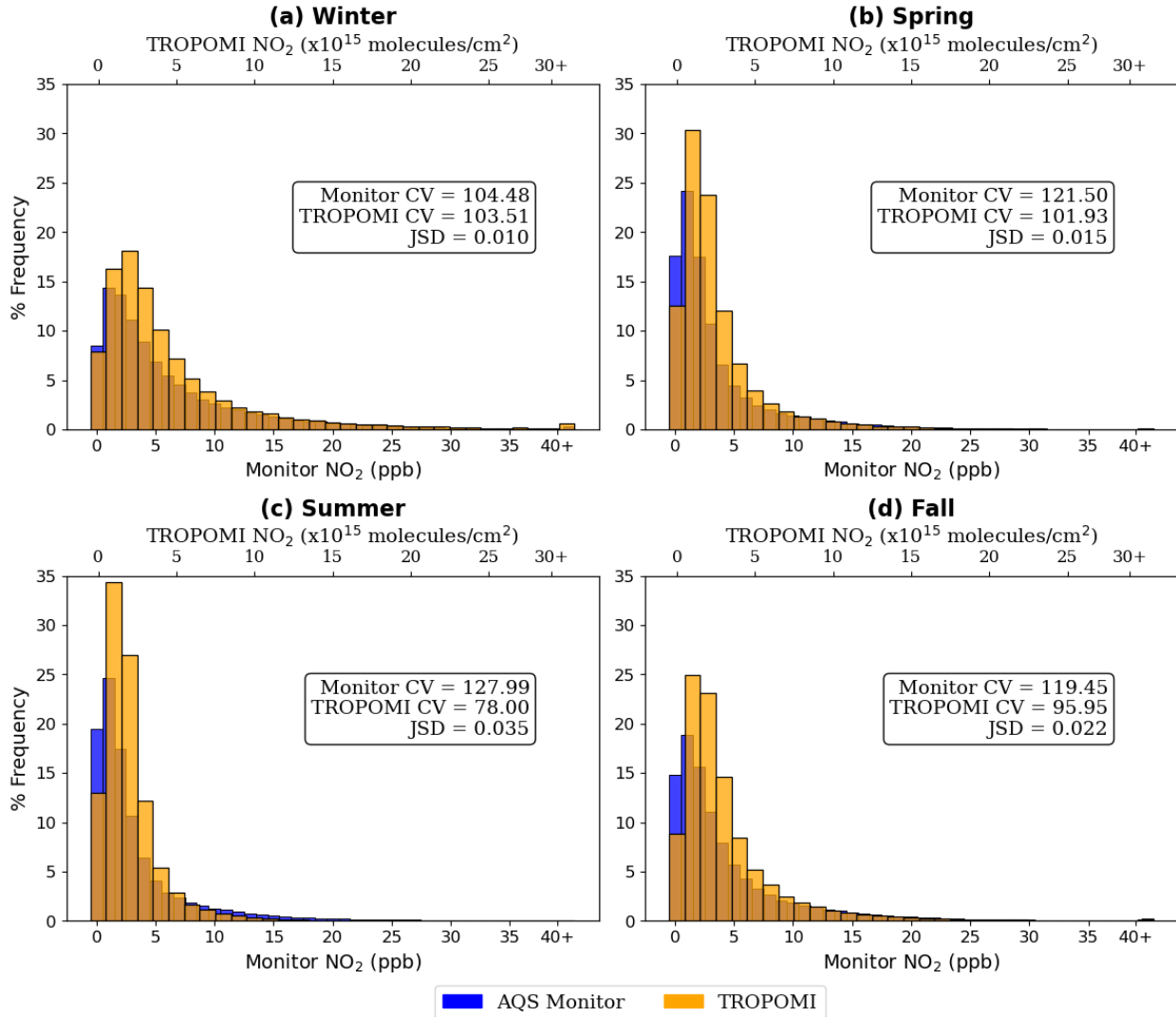
366   Figure 2. Seasonal frequency distributions of 2019-2023 NO2 as measured by AQS ground-based

367   monitors (blue) and TROPOMI (light orange) data for four seasons: a) winter, b) spring, c)

368   summer, and c) fall. The x-axes indicate the range of NO2, with the primary, lower x-axis

369   showing monitor NO2 concentrations in parts per billion (ppb) and the secondary, upper x-axis

370   showing TROPOMI NO2 VCD in 10^{15} molecules per cm^2. The boxes show the Coefficient of

371   Variation (CV; %) and Jensen Shannon Divergence (JSD) for each season.

372   This reduced variability in satellite observations can likely be attributed to the vertical mixing

373   reflected in satellite retrievals, as well as horizontal spatial averaging reflected in satellite data

374   versus point-based NO_2 that are captured by ground monitors. This finding is consistent with

375   previous studies that highlight the spatial averaging nature of satellite-based measurements,

376   which integrate NO_2 amounts over a larger area than the point-based monitors (Ialongo et al.,

377   2020).

378   Across all seasons shown in Fig. 2, JSD values are all low (< 0.1), indicating that TROPOMI

379   may be good at predicting surface NO_2 across seasons. The alignment is strongest in winter (JSD

380   = 0.010), while the divergence is highest in summer (JSD = 0.035), meaning the monitors and

381   TROPOMI align best when the NO_2 lifetime is long in the colder months, and they align the

382   worst when the NO_2 lifetime is short in the warmer months. The better alignment in winter could

383   also be attributed to winter having the largest range of values in the data, which reduces the

384   sensitivity of the JSD calculation to small differences in the distributions. A wider spread in NO_2

385   values means that relative discrepancies between TROPOMI and monitor measurements are

386   smaller in proportion to the total variability, potentially leading to greater similarity.

387   Across seasons, we find that CAPS or "true NO_2" monitors tend to have slightly worse alignment

388   with TROPOMI than traditional, chemiluminescence monitors. Out of the monitors used in this

389   study, 102 were identified as CAPS monitors, and 401 as traditional monitors. In winter, CAPS

390   monitors have a JSD of 0.027 and traditional monitors a JSD of 0.009. In summer, CAPS

391   monitors have a JSD of 0.078 and traditional monitors a JSD of 0.03. With all seasons combined,

392   CAPS monitors have a JSD of 0.047 and traditional monitors have a JSD of 0.016.

393   Table 1 shows the CV and JSD for both monitor and satellite data from 2019 through 2023,

394   aggregated across all seasons and separated by monitor classification (interstate, highway, and

395   non-roadway), where roadway monitors are classified as being within 50 meters (Table 1a) or

396   300 meters (Table 1b) of a road. For the 50-m buffer (Table 1a), the coefficient of variation for

397   ground-based monitor data increases progressively from interstate monitor locations to non-

398   roadway locations, with interstate monitors exhibiting the lowest variability (CV = 75.07%) and

399   non-roadway monitors showing the highest variability (CV = 118.17%). This indicates that NO_2

400   concentrations measured by ground monitors in interstate areas are more consistent compared to

401   non-roadway regions. This pattern is mirrored in the satellite data, with CV values ranging from

402 91.62% for highway monitors to 106.16% for non-roadway monitors. These patterns suggest that

403 regular emissions play a larger role in determining near-road NO_2, where non-road areas vary

404 with changes in wind patterns and the chemical environment.

405 For highway monitors, the CVs of satellite (CV = 91.62%) and monitor data (CV = 96.27%) are

406 similar, indicating that TROPOMI performs similarly to ground monitors in capturing NO_2

407 variability along highways. Near interstates, TROPOMI (CV = 92.60%) may capture more

408 variability than the ground-based measurements (CV = 75.07%), a finding that contrasts with

409 Fig. 1, where TROPOMI shows a narrower range of NO_2 values across all distances. This

410 difference could stem from the fact that the interquartile ranges in Fig. 1 measure the spread of

411 absolute values, while the coefficient of variation accounts for variability relative to the mean.

412 Together, these metrics reveal that TROPOMI may not fully capture localized extremes

413 (narrower IQR) but still captures more relative variability in pollution near interstates than

414 monitors (higher CV).

	Road Type	Monitor CV	TROPOMI CV	JSD	# of Monitors
a) 50-m Buffer	Interstate	75.07	92.60	0.158	58
	Highway	96.27	91.61	0.095	17
	Non-roadway	118.17	106.16	0.009	428
b) 300-m Buffer	Interstate	77.20	91.014	0.133	91
	Highway	135.76	92.31	0.017	90
	Non-roadway	116.23	108.43	0.008	320

415

416 Table 1. Coefficient of variation (%) and Jensen-Shannon divergence for all seasons combined at

417 interstate, highway, and non-roadway monitors 2019-2023 for the 50-m and 300-m roadway

418 buffers.

419 The key differences seen within the JSD across the three monitor classifications are also present

420 in the percent frequency distributions of NO_2 measured by ground-based monitors and

421 TROPOMI (Figure S5), with interstate monitors having the lowest alignment (JSD = 0.158),

422 highway monitors having better alignment (JSD = 0.095), and non-roadway monitors having the

423 best alignment (JSD = 0.009). The strong alignment between TROPOMI and monitor

424 distributions in non-roadway regions is consistent with previous studies (Dressel et al., 2022;

425   Kim et al., 2024; Ialongo et al., 2020). This close alignment may be due to the relatively lower

426   NO_2 concentrations, which TROPOMI captures more accurately compared to regions with

427   higher emissions. These findings further align with previous work showing that TROPOMI tends

428   to underestimate NO_2 in high-pollution areas (such as interstates and highways) but slightly

429   overestimates in areas of lower pollution, such as rural areas (Dressel et al., 2022; Ialongo et al.,

430   2020; Goldberg et al., 2024).

431   Due to the large jump in NO_2 levels seen within Fig. 1 in the 50-300m category, we compare the

432   50-meter buffer roadway classifications (Figure S5; Table 1a) with the 300-meter buffer

433   classifications (Figure S6; Table 1b). Notable differences emerge between distributions,

434   particularly in the highway category, where 73 monitors are added to the highway distribution

435   (increasing from 17 to 90 monitors; Table 1) due to the larger buffer. The alignment between

436   monitor data and TROPOMI observations is significantly improved within the 300-meter buffer

437   near highways. This improvement in alignment is likely due to the decay of NO_2 with increasing

438   distance from the road (Karner et al., 2010; Kimbrough et al., 2017; Richmond-Bryant et al.,

439   2017). Consequently, the lower surface NO_2 concentrations observed at 300 meters are better

440   captured by TROPOMI. This is reflected in Table 1, which shows a substantial reduction in the

441   JSD for highway monitors, from 0.095 in the 50-meter buffer to 0.017 in the 300-meter buffer

442   (an 82% increase in alignment at the 300-meter buffer).

443   The differences observed in the highway category with the 300-meter buffer may be present

444   since the distribution includes 73 more monitors than the 50-meter buffer, capturing lower NO_2

445   amounts that are more aligned with TROPOMI's observations. On the other hand, the interstates

446   category exhibits less noticeable change, with only 33 additional monitors in the 300-meter

447   buffer distribution (increasing from 58 in the 50-meter buffer, Table 1a; to 91 in the 300-meter

448   buffer, Table 1b). This suggests that the monitors added in the 300-meter buffer for interstates

449   measure NO_2 levels similar to those already captured in the 50-meter buffer, resulting in little

450   change to the overall distribution.

451   These results indicate that TROPOMI follows the trend of NO_2 decreasing with increasing

452   distance from roadways that ground-based monitors record, and TROPOMI captures surface

453   concentrations best in winter and at 300+ meters away from the traffic source.

454

3.2 Column-Column Daily Alignment

Here we compare the distributions of NO_2 from TROPOMI and TEMPO with ground-based monitors to assess how well each satellite instrument captures daily variations in NO_2 concentrations. Our results indicate that TEMPO consistently aligns more closely with ground-based measurements than TROPOMI, particularly in high NO_2 areas such as highways and interstates.

Figure 3 shows the distributions of NO_2 as measured by AQS ground-based monitors (filtered to match valid TROPOMI and TEMPO data), TROPOMI, and TEMPO, separated by road classifications (interstates, highways, and non-roadways) for December 2023 and July 2024. The 1 pm and 2 pm UTC (based on time zone) TEMPO and AQS values were averaged to align with the TROPOMI overpass time of ~1:30 pm LT (see Sect. 2.3). The monitor data in each comparison differs due to the data filtering (see Sect. 2.2 and 2.3). The comparison of frequency distributions reveals how well TEMPO and TROPOMI capture the wide range of ground-based monitor readings across these classifications and time periods.

In December 2023, TEMPO (JSD = 0.007) and TROPOMI (JSD = 0.021) exhibit distinct differences in how well they capture NO_2 distributions across the various road classifications. Near interstates, TEMPO has a 90th percentile at 18.34 x 10^{15} molecules/cm^2 whereas the TROPOMI 90th percentile is 11.27 x 10^{15} molecules/cm^2. TEMPO aligns more closely with monitor distributions with a JSD of 0.066 compared to the TROPOMI JSD of 0.145 (Figure 3). TEMPO has 21.42% of data points above 11 x 10^{15} molecules/cm^2 for interstate values in December, whereas TROPOMI appears to underestimate the frequency of higher NO_2 levels more, with a cumulative frequency of 10.53% above that threshold. Near highways, the TEMPO 90th percentile is 14.70 x 10^{15} molecules/cm^2 compared to TROPOMI with a 90th percentile of 10.06 x 10^{15} molecules/cm^2. The JSD for TEMPO is 0.049 and TROPOMI is 0.125 for highway monitors, indicating that TEMPO has much better alignment on highways (Figure 3). For non-roadway locations, both instruments show very good alignment (TEMPO JSD = 0.005; TROPOMI JSD = 0.012; Figure 3) with the monitor data distributions, but with TEMPO again being slightly better.

483   In July 2024, the patterns show greater divergence across road classifications (TEMPO JSD =

484   0.027; TROPOMI JSD = 0.049) between the satellite observations and ground-based monitor

485   data compared to the December 2023 distributions. Near interstates, the TEMPO 90th percentile

486   is 8.46 x 10^{15} molecules/cm^2 and the TROPOMI 90th percentile is 5.58 x 10^{15} molecules/cm^2,

487   with TEMPO aligning more closely (JSD of 0.133 compared to TROPOMI JSD of 0.265; Figure

488   3). TEMPO has 17.01% of data points above 7 x 10^{15} molecules/cm^2 for interstate values in July,

489   whereas TROPOMI appears to underestimate the frequency of higher NO$_2$ levels more, with a

490   cumulative frequency of 3.61% above that threshold. Near highways, TEMPO achieves a much

491   better representation of the higher observed NO$_2$ with a 90th percentile of 9.34 x 10^{15}

492   molecules/cm^2 compared to TROPOMI with a 90th percentile of 5.32 x 10^{15} molecules/cm^2. The

493   JSD for TEMPO is 0.151 and TROPOMI is 0.201 for highway monitors, indicating that TEMPO

494   has better alignment near highways. For non-roadway locations, both instruments show very

495   good alignment (TEMPO JSD = 0.024; TROPOMI JSD = 0.023; Figure 3) with the monitor data

496   distributions, with TEMPO and TROPOMI alignment with ground monitors being more

497   comparable than in December 2023.
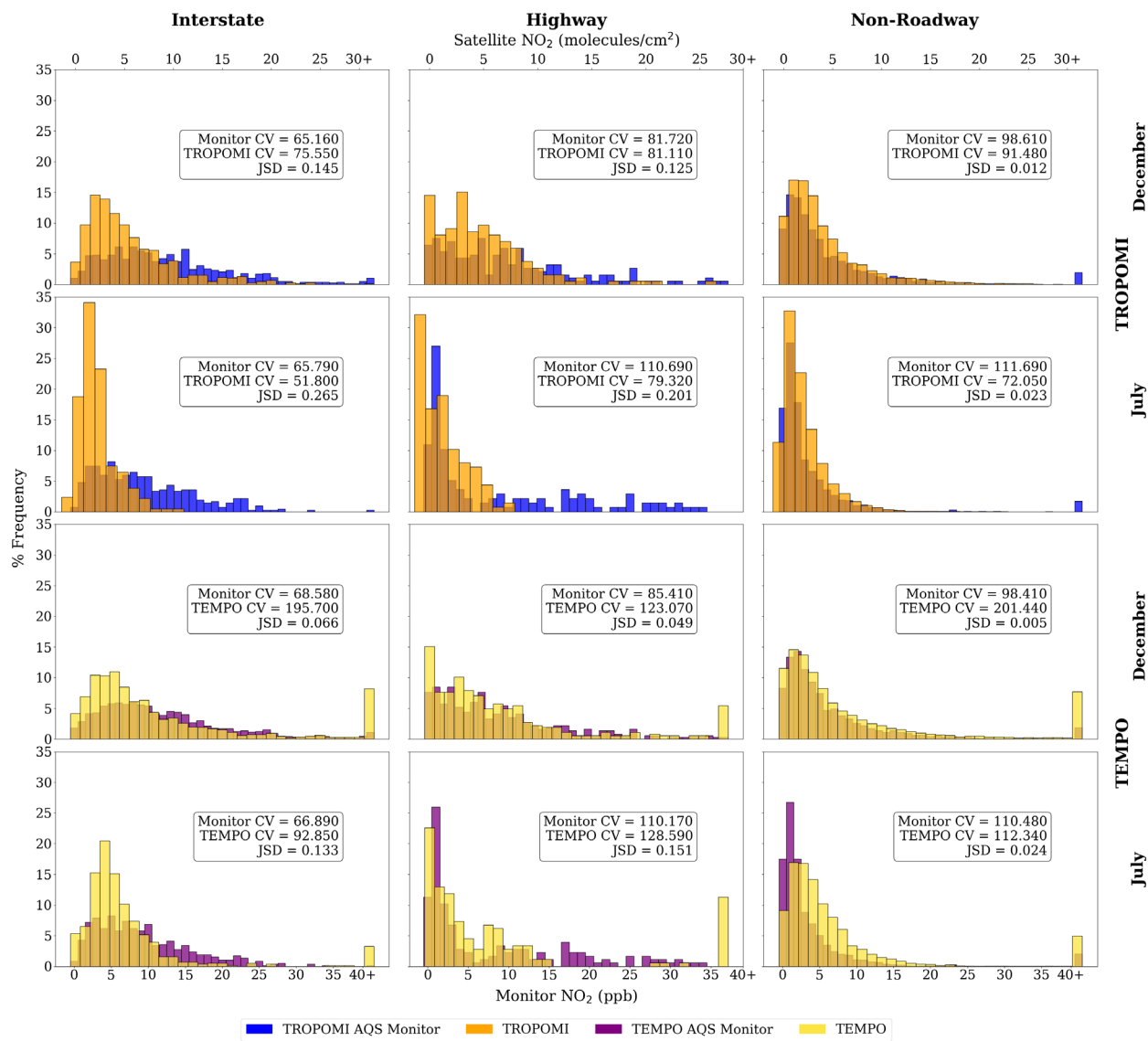
Figure 3. December 2023 and July 2024 at the TROPOMI overpass time (~13:30 LST) frequency distributions of NO₂ as measured by AQS ground-based monitors filtered to the valid TROPOMI (blue) and TEMPO (purple), TROPOMI (light orange), and TEMPO (yellow) data for three monitor classifications: Interstate, Highway, and Non-roadway. The x-axes indicate the range of NO₂, with the primary, lower x-axis showing monitor NO₂ concentrations in parts per billion (ppb) and the secondary, upper x-axis showing TROPOMI NO₂ VCD and TEMPO NO₂ VCD in 10^{15} molecules per cm^2. The boxes show the Coefficient of Variation (CV) and Jensen Shannon Divergence (JSD) for each season and monitor classification.

507 Throughout both December 2023 and July 2024, TEMPO's improved alignment with ground-

508 based monitors compared to TROPOMI may be attributed to several factors. TEMPO operates

509 from a geostationary orbit, allowing it to take hourly measurements and capture the diurnal

510 variability of NO_2 concentrations more effectively than TROPOMI, which has a single daily

511 overpass time. This high temporal resolution enables TEMPO to better match the timing of NO_2

512 peaks and fluctuations detected by ground-based monitors, which are also recorded on an hourly

513 basis. Additionally, TEMPO's finer spatial resolution, approximately 2 km in the north-south

514 direction and 4.5 km in the east-west direction, may allow it to capture more localized pollution

515 sources, such as traffic emissions along highways and interstates. This may be why we see such a

516 large difference in alignment in the interstate and highway categories between TEMPO and

517 TROPOMI, and very little difference in alignment in the non-road category. In contrast,

518 TROPOMI's 4 km x 4 km (re-gridded) resolution and single overpass time may be less effective

519 at capturing these localized variations. TEMPO's finer resolution in one direction and its frequent

520 observations may enable it to more precisely match the spatial and temporal variability detected

521 by ground-based monitors. The consistency of slight underestimation for both instruments in

522 high-pollution areas like highways and interstates suggests challenges in fully capturing elevated

523 NO_2 levels that occur near traffic sources. Overall, this indicates that while TEMPO generally

524 provides a closer approximation of NO_2 distributions compared to TROPOMI, both satellite

525 instruments show limitations, particularly in representing peak concentrations at high-polluting

526 sites.

527

3.3 Column-Surface Diurnal Alignment

529 In this section we explore the hourly alignment between monitor and hourly TEMPO

530 distributions at interstate, highway, and non-roadway monitors. We find that TEMPO aligns best

531 with ground monitors around midday and exhibits poorer alignment in the early morning and

532 early evening.

533 Figure 4 presents the hourly JSD for TEMPO NO_2 measurements compared with ground

534 monitors categorized by interstate (red), highway (orange), and non-roadway (green) monitors

535 for December 2023 (Figure 4a) and July 2024 (Figure 4b). The results highlight distinct diurnal

patterns across road types and seasons, reflecting the influence of traffic emissions, atmospheric mixing, and insolation.

In December 2023, all monitor categories exhibit similar trends in the early morning, with high JSD values (highway JSD = 0.358; interstate JSD = 0.331; non-road JSD = 0.210) indicative of moderate to poor alignment between TEMPO and ground-based monitors. This pattern, consistent with early morning rush hour emissions and limited atmospheric vertical mixing (Harkey and Holloway, 2024) as well as a decrease in TEMPO's measurement accuracy due to high solar zenith angles in the morning according to TEMPO documentation (NASA Langley Research Center, 2024), suggests that TEMPO may not capture rapid increases in NO_2 during high traffic and low mixing periods. By mid-morning, JSD has decreased for all road types (highway JSD = 0.085; interstate JSD = 0.067; non-road JSD = 0.027), indicative of good alignment, with non-road monitors showing the most significant improvement (87% increase in alignment). This pattern of better alignment in non-road monitor areas could be attributed to lower NO_2 levels away from major sources of emissions. As the day progresses in December, JSD values for highway and interstate monitors increase steadily (with highways fluctuating more) after 17 UTC (~12 pm LT), with highways increasing in JSD from 0.102 to 0.490 and interstates increasing from JSD 0.097 to 0.590, indicating worsening alignment in the afternoon and early evening. This pattern may reflect the re-accumulation of NO_2 due to afternoon traffic and the collapse of the boundary layer later in the afternoon (Harkey and Holloway, 2024), as well as the decrease in TEMPO's measurement accuracy in the evening (NASA Langley Research Center, 2024). Non-road monitors show less change in JSD throug the day, suggesting that TEMPO alignment is more consistent in non-road monitor areas throughout the rest of the day, only fluctuating in JSD values between 0.009 and 0.05.

559
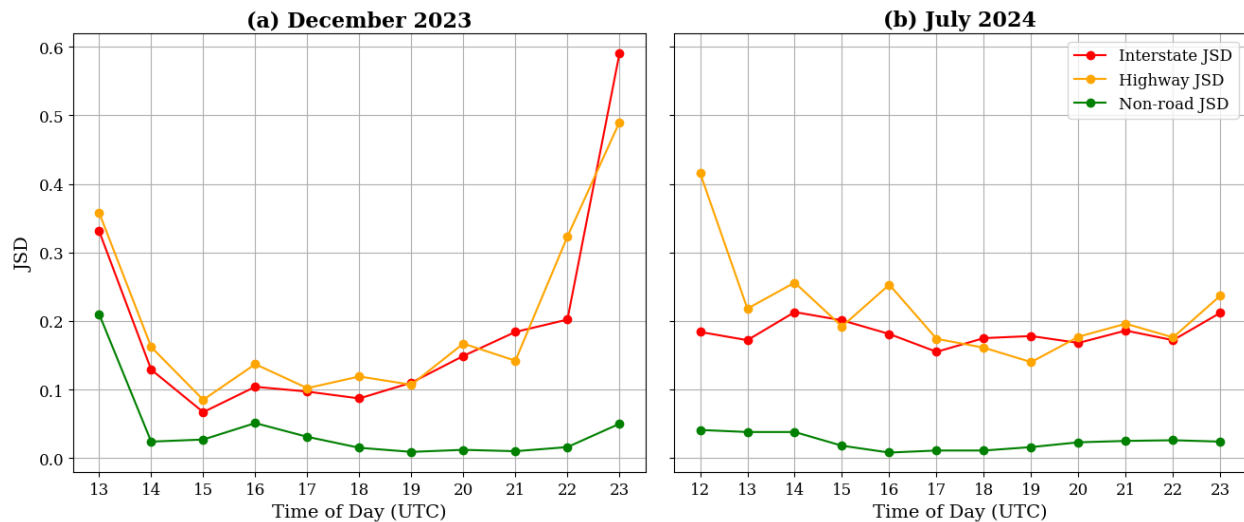
Figure 4. The a) December 2023 and b) July 2024 hourly (UTC) TEMPO NO_2 Jensen-Shannon
Divergences at interstate (red), highway (orange), and non-roadway (green) monitor locations.

560

561

In July 2024 highway and interstate monitors do not exhibit a clear diurnal pattern, with JSD
values fluctuating between 0.14 and 0.416 for highways and 0.155 and 0.212 for interstates
throughout the day. Consistent, localized traffic emissions and the shorter NO_2 lifetime during
the summer suggest a less variable distribution of NO_2. Non-road monitors in July show
somewhat worse alignment in the morning (JSD = 0.041), with improved agreement during the
late morning and early afternoon (JSD ranging between 0.008 and 0.025). The non-road JSD
remains fairly constant into the early evening, with alignment decreasing by about 13%,
indicating that sunlight may play a larger role in the alignment in the evening since the sun is at a
higher position in the sky during this time in the summer than in the winter (which increases in
JSD at this time), enhancing TEMPO's measurement accuracy in the early evening in July.

Both months exhibit their highest JSDs, and worst alignment, in the early morning or early
evening hours, which coincides with peak traffic times and the most uncertainty in TEMPO
observations caused by the solar zenith angle. The best alignment and lowest JSDs occur
sometime near midday (~10 am LT to ~2 pm LT).

The disparity between highways and interstates in TEMPO, where highways generally have the
highest JSD, differs from the pattern seen with TROPOMI, where interstates tended to
consistently exhibit worse alignment. This suggests that TEMPO's higher spatial and temporal

579 resolution may capture localized sources more effectively, leading to variations in alignment

580 based on the distribution and intensity of NO_2 sources.

4 Conclusions

582 This study evaluates the distributional alignment among estimates of NO_2 abundance from

583 TROPOMI, TEMPO, and ground monitors to inform the potential of satellite data for both

584 regulatory and public health applications, particularly in informing future NO_2 monitor siting

585 strategies. Several limitations and sources of uncertainty should be considered. Several

586 limitations of this analysis include: (1) The overrepresentation of AQS monitors in urban areas;

587 (2) the temporal mismatch between satellite and ground measurements; and (3) the distance from

588 roads analysis doesn't consider other local factors. A key limitation is the overrepresentation of

589 urban areas in the AQS monitoring network, which may bias our results toward urban areas.

590 Since AQS monitors are more densely located in urban regions with high emissions and complex

591 local sources, the results may not fully capture alignment in more rural areas with fewer

592 monitoring stations. Another important consideration is the slight temporal mismatch between

593 satellite and ground-based measurements. TROPOMI provides a single daily observation around

594 13:30 pm local solar time, whereas ground monitors and TEMPO record NO_2 concentrations

595 throughout the day. To better align with TROPOMI's overpass, we averaged 1 pm and 2 pm LT

596 TEMPO and ground monitor NO_2 values. Since NO_2 concentrations can change rapidly due to

597 meteorological conditions and emissions variability, this averaging approach may introduce

598 some error in comparisons between TEMPO, TROPOMI, and ground-based measurements. The

599 classification of monitors by distance from roads is based on buffer analysis, which does not

600 account for local factors such as wind direction, terrain, proximity to industry, and traffic density,

601 all of which influence NO_2 dispersion. Despite these uncertainties, our findings highlight patterns

602 in column-surface NO_2 agreement and demonstrate the potential for satellite data to complement

603 ground-based monitoring.

604 The Jensen-Shannon Divergence (JSD) offers a robust and interpretable metric for comparing the

605 alignment and similarity of NO_2 distributions. Its symmetry and bounded range allowed us to

606 evaluate the degree of similarity between satellite and monitor NO_2 values across different

607 spatial and temporal scales, providing a clear quantitative framework for assessing the similarity

608 of two different instruments.

609   Past studies comparing surface and satellite NO_2 have found temporal correlation of daily values

610   at individual sites ranging from r=0.61 to r=0.69 (Lamsal et al., 2014; Lamsal et al., 2015),

611   monthly and seasonal values at individual sites ranging from r=0.67 to r=0.90 (Griffin et al.,

612   2019; Yu & Li, 2022; Harkey & Holloway, 2024; Dressel et al., 2022; Xu & Xiang, 2023;

613   Lamsal et al., 2015), and annual average values at sites ranging from r=0.68 to r=0.93 (Zhang et

614   al., 2018; Lamsal et al., 2015; Goldberg et al., 2021; Kim et al., 2024; Bechle et al., 2013; H. J.

615   Lee et al., 2023). Here, r refers to the Pearson correlation coefficient, which measures the

616   strength and direction of a linear relationship between variables. In some cases, these

617   comparisons adjusted column values to the surface (e.g. Lamsal et al., 2014) and/or adjusted

618   ground-monitors to reduce the error in chemiluminescent detection of NO_2 (e.g. Lamsal et al.,

619   2015; Bechle et al., 2013). Using similar methods, TROPOMI tends to show better agreement

620   with annual AQS NO_2 than does OMI, e.g. r=0.81 using TROPOMI (Goldberg et al., 2015)

621   versus r=0.68 from OMI (Lamsal et al., 2015). Off-road AQS monitors tend to show better

622   agreement with satellite data than near-road AQS monitors, e.g. r = 0.81-0.87 at non-near-road

623   sites versus r = 0.64-0.74 at near-road sites (Kim et al., 2024). The underestimation of estimated

624   near-surface NO_2 near roads and localized sources is a recurring issue in OMI and TROPOMI

625   NO_2 VCDs (Dressel et al., 2022; Goldberg et al., 2024; Ialongo et al., 2020).

626   In this study, we find a pattern of decreasing NO_2 with increasing distance from traffic sources,

627   which is consistent with the findings of previous studies (Kimbrough et al., 2017; Karner et al.,

628   2010; Richmond-Bryant et al., 2017). While ground-based monitors and TROPOMI satellite data

629   may differ with proximity to roadways, particularly within 50-m, their measurements still follow

630   the same overall trend. This convergence with increasing distance may be due to the reduction of

631   localized near-road emissions and the broader atmospheric mixing captured more effectively by

632   satellite observations at greater distances from roads. Using a larger buffer distance from roads

633   (300 meters instead of 50 meters) improves the alignment between TROPOMI and monitor data,

634   especially for highway monitor locations (JSD decreases by ~82%). The overall trend reflects the

635   well-established gradient of declining NO_2 levels with increasing distance from traffic sources,

636   and TROPOMI's ability to capture this trend, even if the specific values differ from AQS

637   monitors in the near-road environment. Our findings indicate that TROPOMI tends to slightly

638   underestimate surface NO_2 concentrations in areas with high traffic, such as interstates and

639   highways, due to its spatial resolution and full-column measurements, which smooth out

640   localized, ground-level pollution peaks captured by ground monitors. This is most evident in

641   interstate monitors, where the JSD reveals the greatest divergence between satellite and monitor

642   data (JSD = 0.158). These results are consistent with prior studies (Dressel et al., 2022; Kim et

643   al., 2024; Ialongo et al., 2020), which also found that satellite instruments are less effective at

644   capturing high NO_2 events near localized sources like traffic. The distributional alignment

645   improves in non-roadway monitors (JSD = 0.009), where NO_2 levels are lower, and there are

646   usually fewer localized sources of pollution. The lower pollution levels in these areas allow

647   TROPOMI to more accurately reflect the conditions captured by ground-based monitors, leading

648   to lower JSD values, and therefore better alignment. This trend suggests that TROPOMI may be

649   particularly useful for monitoring air quality in rural or less polluted regions where ground

650   monitors are sparse or absent.

651   Seasonality plays a critical role in the similarity of satellite and monitor data. Winter consistently

652   shows the best alignment (JSD = 0.010), with the TROPOMI distribution capturing nearly the

653   full gradient of NO_2 seen within the ground-based monitor distribution. This likely reflects the

654   longer atmospheric lifetime of NO_2 in winter, which allows for better vertical mixing and less

655   spatial variability (Harkey et al., 2015; Boersma et al., 2009; Shah et al., 2020). In contrast,

656   summer shows the worst alignment (JSD = 0.035), which is likely due to the shorter lifetime of

657   NO_2 and increased photochemical activity during warmer months, causing greater discrepancies

658   between localized surface measurements and the satellite column. Similar conclusions were

659   reached by previous studies (Shah et al., 2020; Karagkiozidis et al., 2023), indicating that

660   seasonality is a crucial factor in assessing satellite performance for regulatory purposes. These

661   seasonal differences underscore the need for considering temporal factors when evaluating the

662   use of satellite data for monitor siting and NO_2 regulation.

663   The integration of TEMPO data into this study highlights its potential to advance our

664   understanding of NO_2 distributions, especially when compared to TROPOMI. TEMPO's ability

665   to provide hourly measurements at a finer spatial resolution offers significant advantages in

666   capturing diurnal NO_2 patterns and detecting localized pollution events. Our findings from

667   December 2023 and July 2024 at the TROPOMI overpass time (~13:30 LST) demonstrate that

668   TEMPO better captures the wide range of surface NO_2 measurements than TROPOMI,

669   especially at higher NO_2 levels. TEMPO's JSDs are almost always lower than TROPOMI's, with

670   JSDs ranging from 0.005 to 0.151 and TROPOMI's JSDs ranging from 0.012 to 0.265. This

671   improvement in alignment with ground monitors could be attributed to TEMPO's better spatial

672   and temporal resolution.

673   We also find that TEMPO is best at capturing ground-level NO_2 amounts around midday (~10

674   am to ~2 pm LT). This could be due to the lower traffic levels and therefore lower pollution

675   levels during this time period, as well as a lower solar zenith angle, allowing TEMPO to have

676   more accurate measurements. However, challenges remain in completely capturing high NO_2

677   levels during peak traffic times and accurately capturing NO_2 during high solar zenith angles in

678   the morning and evening across monitor classifications. These results underscore the influence of

679   spatial resolution, time of day, and measurement frequency on the ability of satellite instruments

680   to align with ground-based NO_2 measurements. Future research should build upon these insights

681   by incorporating longer time periods and multiple years of data as more TEMPO data becomes

682   available to study long-term TEMPO distributions. The enhanced temporal and spatial resolution

683   of TEMPO, alongside its comparison to other instruments like TROPOMI, provides valuable

684   context for understanding the dynamics of NO_2 pollution, especially how it varies throughout the

685   day. Spatially contiguous satellite products and our analysis of air quality variability offer the

686   potential to support air quality managers and public health analysis.

687

Code and Data Availability

689   All data used in this study are open to the public. Hourly NO_2 data from AQS were obtained

690   from https://aqs.epa.gov/aqsweb/airdata/download_files.html. Copernicus Sentinel 5P Level 2

691   TROPOMI NO_2 data were processed by the ESA, Koninklijk Nederlands Meteorologisch

692   Instituut (KNMI; https://doi.org/10.5270/S5P-s4ljg54), downloaded from the NASA Goddard

693   Earth Sciences Data and Information Center (GES DISC) in January 2021, and gridded using

694   WHIPS (https://sage.nelson.wisc.edu/data-and-models/wisconsin-horizontal-interpolation-

695   program-for-satellites-whips/). TEMPO Level 3 NO_2 data were downloaded from NASA's

696   EarthData Search (https://search.earthdata.nasa.gov/search/granules?p=C2930763263-

697   LARC_CLOUD&pg[0][v]=f&tl=1732652660.361!3!!). The 2021 Primary and Secondary Roads

698   Tiger/Line state-level shapefiles were downloaded from the U.S. Census Bureau

699   (https://www.census.gov/cgi-bin/geo/shapefiles/index.php?year=2021&layergroup=Roads).

700 Since all of our data is publicly available and the methods describe our calculations in detail, we

701 did not make our code publicly available. The Jensen Shannon Divergence was calculated using

702 the *scipy.spatial.distance.jensenshannon* python package.

703

Author Contribution

705 SA and TH conceptualized and designed methodology. MH helped with data curation. SA

706 performed data analysis and visualization and prepared the original draft of the manuscript. All

707 authors contributed to reviewing and editing the manuscript.

708

Competing Interests

710 The authors declare that they have no conflict of interest.

711

Acknowledgements

713 This paper was funded by NASA Grant 80NSSC21K0427 through the Health and Air Quality

714 Applied Sciences Team (HAQAST). We also thank the EPA for providing the Air Quality System

715 data, the Earth Sciences Data and Information Center (GES DISC) for TROPOMI L2 data, the

716 Wisconsin Horizontal Interpolation Program for Satellites (WHIPS) for helping to process and

717 grid TROPOMI data, and NASA Langley Atmospheric Science Data Center Distributed Active

718 Archive Center for providing access to the TEMPO data. The authors acknowledge OpenAI 4o

719 for help with data analysis debugging. We also appreciate valuable comments from Muhammad

720 Omar Nawaz and anonymous reviewers from the public discussion.

721

722

References

724 Achakulwisut, P., Brauer, M., Hystad, P., and Anenberg, S. C.: Global, national, and urban

725 burdens of paediatric asthma incidence attributable to ambient NO2 pollution: estimates from

726 global datasets, The Lancet Planetary Health, 3, e166–e178, https://doi.org/10.1016/S2542-

727 5196(19)30046-4, 2019.

728   Aerts, S., Haesbroeck, G., and Ruwet, C.: Multivariate coefficients of variation: Comparison and

729   influence functions, Journal of Multivariate Analysis, 142, 183–198,

730   https://doi.org/10.1016/j.jmva.2015.08.006, 2015.

731   Ahmed, Z., Zeeshan, S., Persaud, N., Degroat, W., Abdelhalim, H., and Liang, B. T.:

732   Investigating genes associated with cardiovascular disease among heart failure patients for

733   translational research and precision medicine, Clinical and Translational Dis, 3, e206,

734   https://doi.org/10.1002/ctd2.206, 2023.

735   Anenberg, S. C., Mohegh, A., Goldberg, D. L., Kerr, G. H., Brauer, M., Burkart, K., Hystad, P.,

736   Larkin, A., Wozniak, S., and Lamsal, L.: Long-term trends in urban NO2 concentrations and

737   associated paediatric asthma incidence: estimates from global datasets, The Lancet Planetary

738   Health, 6, e49–e58, https://doi.org/10.1016/S2542-5196(21)00255-2, 2022.

739   Bai, L., Chen, H., Hatzopoulou, M., Jerrett, M., Kwong, J. C., Burnett, R. T., Van Donkelaar, A.,

740   Copes, R., Martin, R. V., Van Ryswyk, K., Lu, H., Kopp, A., and Weichenthal, S.: Exposure to

741   Ambient Ultrafine Particles and Nitrogen Dioxide and Incident Hypertension and Diabetes:,

742   Epidemiology, 29, 323–332, https://doi.org/10.1097/EDE.0000000000000798, 2018.

743   Bechle, M. J., Millet, D. B., and Marshall, J. D.: Remote sensing of exposure to NO2: Satellite

744   versus ground-based measurement in a large urban area, Atmospheric Environment, 69, 345–

745   353, https://doi.org/10.1016/j.atmosenv.2012.11.046, 2013.

746   Behera, S. N. and Sharma, M.: Transformation of atmospheric ammonia and acid gases into

747   components of PM2.5: an environmental chamber study, Environ Sci Pollut Res, 19, 1187–1197,

748   https://doi.org/10.1007/s11356-011-0635-9, 2012.

749   Boersma, K. F., Jacob, D. J., Trainic, M., Rudich, Y., DeSmedt, I., Dirksen, R., and Eskes, H. J.:

750   Validation of urban NO$_2$ concentrations and their diurnal and seasonal

751   variations observed from the SCIAMACHY and OMI sensors using in situ surface

752   measurements in Israeli cities, Atmos. Chem. Phys., 9, 3867–3879, https://doi.org/10.5194/acp-

753   9-3867-2009, 2009.

754   Boersma, K. F., Eskes, H. J., Richter, A., De Smedt, I., Lorente, A., Beirle, S., Van Geffen, J. H.

755   G. M., Zara, M., Peters, E., Van Roozendael, M., Wagner, T., Maasakkers, J. D., Van Der A, R. J.,

756 Nightingale, J., De Rudder, A., Irie, H., Pinardi, G., Lambert, J.-C., and Compernolle, S. C.:

757 Improving algorithms and uncertainty estimates for satellite NO_2

758 retrievals: results from the quality assurance for the essential climate variables (QA4ECV)

759 project, Atmos. Meas. Tech., 11, 6651–6678, https://doi.org/10.5194/amt-11-6651-2018, 2018.

760 Camilleri, S. F., Kerr, G. H., Anenberg, S. C., and Horton, D. E.: All-Cause NO_2 -Attributable

761 Mortality Burden and Associated Racial and Ethnic Disparities in the United States, Environ.

762 Sci. Technol. Lett., 10, 1159–1164, https://doi.org/10.1021/acs.estlett.3c00500, 2023.

763 Wisconsin Horizontal Interpolation Program for Satellites (WHIPS):

764 https://sage.nelson.wisc.edu/data-and-models/wisconsin-horizontal-interpolation-program-for-

765 satellites-whips/, last access: 6 December 2024.

766 Chance, K., Liu, X., Miller, C. C., González Abad, G., Huang, G., Nowlan, C., Souri, A.,

767 Suleiman, R., Sun, K., Wang, H., Zhu, L., Zoogman, P., Al-Saadi, J., Antuña-Marrero, J.-C., Carr,

768 J., Chatfield, R., Chin, M., Cohen, R., Edwards, D., Fishman, J., Flittner, D., Geddes, J., Grutter,

769 M., Herman, J. R., Jacob, D. J., Janz, S., Joiner, J., Kim, J., Krotkov, N. A., Lefer, B., Martin, R.

770 V., Mayol-Bracero, O. L., Naeger, A., Newchurch, M., Pfister, G. G., Pickering, K., Pierce, R. B.,

771 Rivera Cárdenas, C., Saiz-Lopez, A., Simpson, W., Spinei, E., Spurr, R. J. D., Szykman, J. J.,

772 Torres, O., and Wang, J.: TEMPO Green Paper: Chemistry, physics, and meteorology

773 experiments with the Tropospheric Emissions: monitoring of pollution instrument, in: Sensors,

774 Systems, and Next-Generation Satellites XXIII, Sensors, Systems, and Next-Generation

775 Satellites XXIII, Strasbourg, France, 10, https://doi.org/10.1117/12.2534883, 2019.

776 Chowdhury, S., Haines, A., Klingmüller, K., Kumar, V., Pozzer, A., Venkataraman, C., Witt, C.,

777 and Lelieveld, J.: Global and national assessment of the incidence of asthma in children and

778 adolescents from major sources of ambient NO_2, Environ. Res. Lett., 16, 035020,

779 https://doi.org/10.1088/1748-9326/abe909, 2021.

780 Clim, A., Zota, R. D., and TinicĂ, G.: The Kullback-Leibler Divergence Used in Machine

781 Learning Algorithms for Health Care Applications and Hypertension Prediction: A Literature

782 Review, Procedia Computer Science, 141, 448–453, https://doi.org/10.1016/j.procs.2018.10.144,

783 2018.

Cooper, M. J., Martin, R. V., McLinden, C. A., and Brook, J. R.: Inferring ground-level nitrogen dioxide concentrations at fine spatial resolution applied to the TROPOMI satellite instrument, Environ. Res. Lett., 15, 104013, https://doi.org/10.1088/1748-9326/aba3a5, 2020.

Dang, R., Jacob, D. J., Shah, V., Eastham, S. D., Fritz, T. M., Mickley, L. J., Liu, T., Wang, Y., and Wang, J.: Background nitrogen dioxide (NO_2) over the United States and its implications for satellite observations and trends: effects of nitrate photolysis, aircraft, and open fires, Atmos. Chem. Phys., 23, 6271–6284, https://doi.org/10.5194/acp-23-6271-2023, 2023.

Dressel, I. M., Demetillo, M. A. G., Judd, L. M., Janz, S. J., Fields, K. P., Sun, K., Fiore, A. M., McDonald, B. C., and Pusede, S. E.: Daily Satellite Observations of Nitrogen Dioxide Air Pollution Inequality in New York City, New York and Newark, New Jersey: Evaluation and Application, Environ. Sci. Technol., 56, 15298–15311, https://doi.org/10.1021/acs.est.2c02828, 2022.

Duncan, B. N., Yoshida, Y., De Foy, B., Lamsal, L. N., Streets, D. G., Lu, Z., Pickering, K. E., and Krotkov, N. A.: The observed response of Ozone Monitoring Instrument (OMI) NO2 columns to NOx emission controls on power plants in the United States: 2005–2011, Atmospheric Environment, 81, 102–111, https://doi.org/10.1016/j.atmosenv.2013.08.068, 2013.

Duncan, B. N., Prados, A. I., Lamsal, L. N., Liu, Y., Streets, D. G., Gupta, P., Hilsenrath, E., Kahn, R. A., Nielsen, J. E., Beyersdorf, A. J., Burton, S. P., Fiore, A. M., Fishman, J., Henze, D. K., Hostetler, C. A., Krotkov, N. A., Lee, P., Lin, M., Pawson, S., Pfister, G., Pickering, K. E., Pierce, R. B., Yoshida, Y., and Ziemba, L. D.: Satellite data of atmospheric pollution for U.S. air quality applications: Examples of applications, summary of data end-user resources, answers to FAQs, and common mistakes to avoid, Atmospheric Environment, 94, 647–662, https://doi.org/10.1016/j.atmosenv.2014.05.061, 2014.

Dunlea, E. J., Herndon, S. C., Nelson, D. D., Volkamer, R. M., San Martini, F., Sheehy, P. M., Zahniser, M. S., Shorter, J. H., Wormhoudt, J. C., Lamb, B. K., Allwine, E. J., Gaffney, J. S., Marley, N. A., Grutter, M., Marquez, C., Blanco, S., Cardenas, B., Retama, A., Ramos Villegas, C. R., Kolb, C. E., Molina, L. T., and Molina, M. J.: Evaluation of nitrogen dioxide chemiluminescence monitors in a polluted urban environment, Atmos. Chem. Phys., 7, 2691–2704, https://doi.org/10.5194/acp-7-2691-2007, 2007.

813   AirData Pre-Generated Hourly File Downloads:

814   https://aqs.epa.gov/aqsweb/airdata/download_files.html#Raw, last access: 21 February 2025.

815   European Space Agency: TROPOMI Level 2 Nitrogen Dioxide, https://doi.org/10.5270/S5P-

816   9bnp8q8, 2021.

817   Fontijn, Arthur., Sabadell, A. J., and Ronco, R. J.: Homogeneous chemiluminescent measurement

818   of nitric oxide with ozone. Implications for continuous selective monitoring of gaseous air

819   pollutants, Anal. Chem., 42, 575–579, https://doi.org/10.1021/ac60288a034, 1970.

820   Frost, G. J., McKeen, S. A., Trainer, M., Ryerson, T. B., Neuman, J. A., Roberts, J. M., Swanson,

821   A., Holloway, J. S., Sueper, D. T., Fortin, T., Parrish, D. D., Fehsenfeld, F. C., Flocke, F.,

822   Peckham, S. E., Grell, G. A., Kowal, D., Cartwright, J., Auerbach, N., and Habermann, T.:

823   Effects of changing power plant NO_x emissions on ozone in the eastern United States: Proof of

824   concept, J. Geophys. Res., 111, 2005JD006354, https://doi.org/10.1029/2005JD006354, 2006.

825   Gantt, B., Owen, R. C., and Watkins, N.: Characterizing Nitrogen Oxides and Fine Particulate

826   Matter near Major Highways in the United States Using the National Near-Road Monitoring

827   Network, Environ. Sci. Technol., 55, 2831–2838, https://doi.org/10.1021/acs.est.0c05851, 2021.

828   Ge, B., Sun, Y., Liu, Y., Dong, H., Ji, D., Jiang, Q., Li, J., and Wang, Z.: Nitrogen dioxide

829   measurement by cavity attenuated phase shift spectroscopy (CAPS) and implications in ozone

830   production efficiency and nitrate formation in Beijing, China, JGR Atmospheres, 118, 9499–

831   9509, https://doi.org/10.1002/jgrd.50757, 2013.

832   Goldberg, D. L., Anenberg, S. C., Kerr, G. H., Mohegh, A., Lu, Z., and Streets, D. G.:

833   TROPOMI NO_2 in the United States: A Detailed Look at the Annual Averages, Weekly Cycles,

834   Effects of Temperature, and Correlation With Surface NO_2 Concentrations, Earth's Future, 9,

835   e2020EF001665, https://doi.org/10.1029/2020EF001665, 2021.

836   Goldberg, D. L., Tao, M., Kerr, G. H., Ma, S., Tong, D. Q., Fiore, A. M., Dickens, A. F.,

837   Adelman, Z. E., and Anenberg, S. C.: Evaluating the spatial patterns of U.S. urban NOx

838   emissions using TROPOMI NO2, Remote Sensing of Environment, 300, 113917,

839   https://doi.org/10.1016/j.rse.2023.113917, 2024.

840   Griffin, D., Zhao, X., McLinden, C. A., Boersma, F., Bourassa, A., Dammers, E., Degenstein, D.,

841   Eskes, H., Fehr, L., Fioletov, V., Hayden, K., Kharol, S. K., Li, S., Makar, P., Martin, R. V.,

842   Mihele, C., Mittermeier, R. L., Krotkov, N., Sneep, M., Lamsal, L. N., Linden, M. T., Geffen, J.

843   V., Veefkind, P., and Wolde, M.: High-Resolution Mapping of Nitrogen Dioxide With

844   TROPOMI: First Results and Validation Over the Canadian Oil Sands, Geophysical Research

845   Letters, 46, 1049–1060, https://doi.org/10.1029/2018GL081095, 2019.

846   Grulke, N. E. and Heath, R. L.: Ozone effects on plants in natural ecosystems, Plant Biol J, 22,

847   12–37, https://doi.org/10.1111/plb.12971, 2020.

848   Hales, S., Atkinson, J., Metcalfe, J., Kuschel, G., and Woodward, A.: Long term exposure to air

849   pollution, mortality and morbidity in New Zealand: Cohort study, Science of The Total

850   Environment, 801, 149660, https://doi.org/10.1016/j.scitotenv.2021.149660, 2021.

851   Harkey, M. and Holloway, T.: Simulated Surface-Column NO_2 Connections for Satellite

852   Applications, JGR Atmospheres, 129, e2024JD041912, https://doi.org/10.1029/2024JD041912,

853   2024.

854   Harkey, M., Holloway, T., Oberman, J., and Scotty, E.: An evaluation of CMAQ NO_2 using

855   observed chemistry-meteorology correlations, JGR Atmospheres, 120,

856   https://doi.org/10.1002/2015JD023316, 2015.

857   Harkey, M., Holloway, T., Kim, E. J., Baker, K. R., and Henderson, B.: Satellite Formaldehyde to

858   Support Model Evaluation, JGR Atmospheres, 126, e2020JD032881,

859   https://doi.org/10.1029/2020JD032881, 2021.

860   Holloway, T., Miller, D., Anenberg, S., Diao, M., Duncan, B., Fiore, A. M., Henze, D. K., Hess,

861   J., Kinney, P. L., Liu, Y., Neu, J. L., O'Neill, S. M., Odman, M. T., Pierce, R. B., Russell, A. G.,

862   Tong, D., West, J. J., and Zondlo, M. A.: Satellite Monitoring for Air Quality and Health, Annu.

863   Rev. Biomed. Data Sci., 4, 417–447, https://doi.org/10.1146/annurev-biodatasci-110920-093120,

864   2021.

865   Huangfu, P. and Atkinson, R.: Long-term exposure to NO2 and O3 and all-cause and respiratory

866   mortality: A systematic review and meta-analysis, Environment International, 144, 105998,

867   https://doi.org/10.1016/j.envint.2020.105998, 2020.

Huber, D. E., Steiner, A. L., and Kort, E. A.: Daily Cropland Soil NO_x Emissions Identified by TROPOMI and SMAP, Geophysical Research Letters, 47, e2020GL089949, https://doi.org/10.1029/2020GL089949, 2020.

Ialongo, I., Virta, H., Eskes, H., Hovila, J., and Douros, J.: Comparison of TROPOMI/Sentinel-5 Precursor NO_2 observations with ground-based measurements in Helsinki, Atmos. Meas. Tech., 13, 205–218, https://doi.org/10.5194/amt-13-205-2020, 2020.

Jia, M., Wang, Z., Wang, C., Mao, D., and Zhang, Y.: A New Vegetation Index to Detect Periodically Submerged Mangrove Forest Using Single-Tide Sentinel-2 Imagery, Remote Sensing, 11, 2043, https://doi.org/10.3390/rs11172043, 2019.

Jones, D. C., Danaher, P., Kim, Y., Beechem, J. M., Gottardo, R., and Newell, E. W.: An information theoretic approach to detecting spatially varying genes, Cell Reports Methods, 3, 100507, https://doi.org/10.1016/j.crmeth.2023.100507, 2023.

Kang, D. and Pickering, K.: Lightning NOx Emissions and the Implications for Surface Air Quality over the Contiguous United States, EM (Pittsburgh Pa), 11, 1–6, 2018.

Karagkiozidis, D., Koukouli, M.-E., Bais, A., Balis, D., and Tzoumaka, P.: Assessment of the NO2 Spatio-Temporal Variability over Thessaloniki, Greece, Using MAX-DOAS Measurements and Comparison with S5P/TROPOMI Observations, Applied Sciences, 13, 2641, https://doi.org/10.3390/app13042641, 2023.

Karner, A. A., Eisinger, D. S., and Niemeier, D. A.: Near-Roadway Air Quality: Synthesizing the Findings from Real-World Data, Environ. Sci. Technol., 44, 5334–5344, https://doi.org/10.1021/es100008x, 2010.

Kebabian, P. L., Herndon, S. C., and Freedman, A.: Detection of Nitrogen Dioxide by Cavity Attenuated Phase Shift Spectroscopy, Anal. Chem., 77, 724–728, https://doi.org/10.1021/ac048715y, 2005.

Kerr, G. H., Goldberg, D. L., Harris, M. H., Henderson, B. H., Hystad, P., Roy, A., and Anenberg, S. C.: Ethnoracial Disparities in Nitrogen Dioxide Pollution in the United States: Comparing Data Sets from Satellites, Models, and Monitors, Environ. Sci. Technol., 57, 19532–19544, https://doi.org/10.1021/acs.est.3c03999, 2023.

Kibirige, G. W., Huang, C. C., Liu, C. L., and Chen, M. C.: Influence of land-sea breeze on PM$_{2.5}$ prediction in central and southern Taiwan using composite neural network, Sci Rep, 13, 3827, https://doi.org/10.1038/s41598-023-29845-w, 2023.

Kim, E. J., Holloway, T., Kokandakar, A., Harkey, M., Elkins, S., Goldberg, D. L., and Heck, C.: A Comparison of Regression Methods for Inferring Near-Surface NO_2 With Satellite Data, JGR Atmospheres, 129, e2024JD040906, https://doi.org/10.1029/2024JD040906, 2024.

Kim, H. C., Kim, S., Lee, S.-H., Kim, B.-U., and Lee, P.: Fine-Scale Columnar and Surface NOx Concentrations over South Korea: Comparison of Surface Monitors, TROPOMI, CMAQ and CAPSS Inventory, Atmosphere, 11, 101, https://doi.org/10.3390/atmos11010101, 2020.

Kim, M., Brunner, D., and Kuhlmann, G.: Importance of satellite observations for high-resolution mapping of near-surface NO2 by machine learning, Remote Sensing of Environment, 264, 112573, https://doi.org/10.1016/j.rse.2021.112573, 2021.

Kimbrough, S., Chris Owen, R., Snyder, M., and Richmond-Bryant, J.: NO to NO2 conversion rate analysis and implications for dispersion model chemistry methods using Las Vegas, Nevada near-road field measurements, Atmospheric Environment, 165, 23–34, https://doi.org/10.1016/j.atmosenv.2017.06.027, 2017.

Knox, J. B. and Lange, R.: Surface Air Pollutant Concentration Frequency Distributions: Implications for Urban Modeling, Journal of the Air Pollution Control Association, 24, 48–53, https://doi.org/10.1080/00022470.1974.10469893, 1974.

Lamsal, L. N., Krotkov, N. A., Celarier, E. A., Swartz, W. H., Pickering, K. E., Bucsela, E. J., Gleason, J. F., Martin, R. V., Philip, S., Irie, H., Cede, A., Herman, J., Weinheimer, A., Szykman, J. J., and Knepp, T. N.: Evaluation of OMI operational standard NO_2 column retrievals using in situ and surface-based NO_2 observations, Atmos. Chem. Phys., 14, 11587–11609, https://doi.org/10.5194/acp-14-11587-2014, 2014.

Lamsal, L. N., Duncan, B. N., Yoshida, Y., Krotkov, N. A., Pickering, K. E., Streets, D. G., and Lu, Z.: U.S. NO2 trends (2005–2013): EPA Air Quality System (AQS) data versus improved observations from the Ozone Monitoring Instrument (OMI), Atmospheric Environment, 110, 130–143, https://doi.org/10.1016/j.atmosenv.2015.03.055, 2015.

924 Lange, K., Richter, A., and Burrows, J. P.: Variability of nitrogen oxide emission fluxes and

925 lifetimes estimated from Sentinel-5P TROPOMI observations, Atmos. Chem. Phys., 22, 2745–

926 2767, https://doi.org/10.5194/acp-22-2745-2022, 2022.

927 Lee, H. J. and Koutrakis, P.: Daily Ambient NO_2 Concentration Predictions Using Satellite

928 Ozone Monitoring Instrument NO_2 Data and Land Use Regression, Environ. Sci. Technol.,

929 140204134232009, https://doi.org/10.1021/es404845f, 2014.

930 Lee, H. J., Liu, Y., and Chatfield, R. B.: Neighborhood-scale ambient NO2 concentrations using

931 TROPOMI NO2 data: Applications for spatially comprehensive exposure assessment, Science of

932 The Total Environment, 857, 159342, https://doi.org/10.1016/j.scitotenv.2022.159342, 2023.

933 Lee, M., Heikes, B. G., Jacob, D. J., Sachse, G., and Anderson, B.: Hydrogen peroxide, organic

934 hydroperoxide, and formaldehyde as primary pollutants from biomass burning, J. Geophys. Res.,

935 102, 1301–1309, https://doi.org/10.1029/96JD01709, 1997.

936 Levinson, R. and Akbari, H.: Potential benefits of cool roofs on commercial buildings:

937 conserving energy, saving money, and reducing emission of greenhouse gases and air pollutants,

938 Energy Efficiency, 3, 53–109, https://doi.org/10.1007/s12053-008-9038-2, 2010.

939 Li, J., Wang, Y., Zhang, R., Smeltzer, C., Weinheimer, A., Herman, J., Boersma, K. F., Celarier,

940 E. A., Long, R. W., Szykman, J. J., Delgado, R., Thompson, A. M., Knepp, T. N., Lamsal, L. N.,

941 Janz, S. J., Kowalewski, M. G., Liu, X., and Nowlan, C. R.: Comprehensive evaluations of

942 diurnal NO₂ measurements during DISCOVER-AQ 2011: effects of

943 resolution-dependent representation of NO_{<i>x</i>}

944 emissions, Atmos. Chem. Phys., 21, 11133–11160, https://doi.org/10.5194/acp-21-11133-2021,

945 2021.

946 Liu, X., Yi, G., Zhou, X., Zhang, T., Lan, Y., Yu, D., Wen, B., and Hu, J.: Atmospheric NO2

947 Distribution Characteristics and Influencing Factors in Yangtze River Economic Belt: Analysis of

948 the NO2 Product of TROPOMI/Sentinel-5P, Atmosphere, 12, 1142,

949 https://doi.org/10.3390/atmos12091142, 2021.

950 Melville, P., Yang, S.M., Saar-Tsechansky, M., Mooney, R.J.: Active Learning for Probability

951 Estimation using Jensen-Shannon Divergence, in: Proceedings of the 16th European Conference

952 on Machine Learning, 268–279, 2005.

953 Menéndez, M. L., Pardo, J. A., Pardo, L., and Pardo, M. C.: The Jensen-Shannon divergence,

954 Journal of the Franklin Institute, 334, 307–318, https://doi.org/10.1016/S0016-0032(96)00063-4,

955 1997.

956 Meng, X., Liu, C., Chen, R., Sera, F., Vicedo-Cabrera, A. M., Milojevic, A., Guo, Y., Tong, S.,

957 Coelho, M. D. S. Z. S., Saldiva, P. H. N., Lavigne, E., Correa, P. M., Ortega, N. V., Osorio, S.,

958 Garcia, Kyselý, J., Urban, A., Orru, H., Maasikmets, M., Jaakkola, J. J. K., Ryti, N., Huber, V.,

959 Schneider, A., Katsouyanni, K., Analitis, A., Hashizume, M., Honda, Y., Ng, C. F. S., Nunes, B.,

960 Teixeira, J. P., Holobaca, I. H., Fratianni, S., Kim, H., Tobias, A., Íñiguez, C., Forsberg, B.,

961 Åström, C., Ragettli, M. S., Guo, Y.-L. L., Pan, S.-C., Li, S., Bell, M. L., Zanobetti, A., Schwartz,

962 J., Wu, T., Gasparrini, A., and Kan, H.: Short term associations of ambient nitrogen dioxide with

963 daily total, cardiovascular, and respiratory mortality: multilocation analysis in 398 cities, BMJ,

964 n534, https://doi.org/10.1136/bmj.n534, 2021.

965 Mills, I. C., Atkinson, R. W., Kang, S., Walton, H., and Anderson, H. R.: Quantitative systematic

966 review of the associations between short-term exposure to nitrogen dioxide and mortality and

967 hospital admissions, BMJ Open, 5, e006946, https://doi.org/10.1136/bmjopen-2014-006946,

968 2015.

969 Mölter, A., Agius, R., De Vocht, F., Lindley, S., Gerrard, W., Custovic, A., and Simpson, A.:

970 Effects of long-term exposure to PM_{10} and NO_2 on asthma and wheeze in a prospective birth

971 cohort, J Epidemiol Community Health, 68, 21–28, https://doi.org/10.1136/jech-2013-202681,

972 2014.

973 Mondal, A., Sharma, S. K., Mandal, T. K., Girach, I., and Ojha, N.: Frequency distribution of

974 pollutant concentrations over Indian megacities impacted by the COVID-19 lockdown, Environ

975 Sci Pollut Res, 29, 85676–85687, https://doi.org/10.1007/s11356-021-16874-z, 2022.

976 Naeger, A. R., Newchurch, M. J., Moore, T., Chance, K., Liu, X., Alexander, S., Murphy, K., and

977 Wang, B.: Revolutionary Air-Pollution Applications from Future Tropospheric Emissions:

Monitoring of Pollution (TEMPO) Observations, Bulletin of the American Meteorological Society, 102, E1735–E1741, https://doi.org/10.1175/BAMS-D-21-0050.1, 2021.

Tropospheric Emissions: Monitoring of Pollution (EVI-1) | NASA's Earth Observing System: https://eospso.nasa.gov/missions/tropospheric-emissions-monitoring-pollution-evi-1, last access: 26 November 2024.

NASA Langley Research Center: TEMPO Level 2/3 trace gas and cloud data user guide, 2024.

Novotny, E. V., Bechle, M. J., Millet, D. B., and Marshall, J. D.: National Satellite-Based Land-Use Regression: NO_2 in the United States, Environ. Sci. Technol., 45, 4407–4414, https://doi.org/10.1021/es103578x, 2011.

Orellano, P., Reynoso, J., Quaranta, N., Bardach, A., and Ciapponi, A.: Short-term exposure to particulate matter (PM10 and PM2.5), nitrogen dioxide (NO2), and ozone (O3) and all-cause and cause-specific mortality: Systematic review and meta-analysis, Environment International, 142, 105876, https://doi.org/10.1016/j.envint.2020.105876, 2020.

Penn, E. and Holloway, T.: Evaluating current satellite capability to observe diurnal change in nitrogen oxides in preparation for geostationary satellite missions, Environ. Res. Lett., 15, 034038, https://doi.org/10.1088/1748-9326/ab6b36, 2020.

Pollack, R.: Studies of Pollutant Concentration Frequency Distributions, 1975.

Qin, M., Yu, H., Hu, Y., Russell, A. G., Odman, M. T., Doty, K., Pour-Biazar, A., McNider, R. T., and Knipping, E.: Improving ozone simulations in the Great Lakes Region: The role of emissions, chemistry, and dry deposition, Atmospheric Environment, 202, 167–179, https://doi.org/10.1016/j.atmosenv.2019.01.025, 2019.

Richmond-Bryant, J., Chris Owen, R., Graham, S., Snyder, M., McDow, S., Oakes, M., and Kimbrough, S.: Estimation of on-road NO2 concentrations, NO2/NOX ratios, and related roadway gradients from near-road monitoring data, Air Qual Atmos Health, 10, 611–625, https://doi.org/10.1007/s11869-016-0455-7, 2017.

Richter, A., Burrows, J. P., Nüß, H., Granier, C., and Niemeier, U.: Increase in tropospheric nitrogen dioxide over China observed from space, Nature, 437, 129–132, https://doi.org/10.1038/nature04092, 2005.

1006 Sangkham, S., Phairuang, W., Sherchan, S. P., Pansakun, N., Munkong, N., Sarndhong, K.,

1007 Islam, Md. A., and Sakunkoo, P.: An update on adverse health effects from exposure to PM2.5,

1008 Environmental Advances, 18, 100603, https://doi.org/10.1016/j.envadv.2024.100603, 2024.

1009 Saurette, D. D., Heck, R. J., Gillespie, A. W., Berg, A. A., and Biswas, A.: Divergence metrics for

1010 determining optimal training sample size in digital soil mapping, Geoderma, 436, 116553,

1011 https://doi.org/10.1016/j.geoderma.2023.116553, 2023.

1012 Shah, V., Jacob, D. J., Li, K., Silvern, R. F., Zhai, S., Liu, M., Lin, J., and Zhang, Q.: Effect of

1013 changing NO_{<i>x</i>} lifetime on the seasonality and long-

1014 term trends of satellite-observed tropospheric NO₂ columns over China,

1015 Atmos. Chem. Phys., 20, 1483–1495, https://doi.org/10.5194/acp-20-1483-2020, 2020.

1016 Sharma, S., Chandra, M., and Kota, S. H.: Health Effects Associated with PM2.5: a Systematic

1017 Review, Curr Pollution Rep, 6, 345–367, https://doi.org/10.1007/s40726-020-00155-3, 2020.

1018 Shetty, S., Schneider, P., Stebel, K., David Hamer, P., Kylling, A., and Koren Berntsen, T.:

1019 Estimating surface NO2 concentrations over Europe using Sentinel-5P TROPOMI observations

1020 and Machine Learning, Remote Sensing of Environment, 312, 114321,

1021 https://doi.org/10.1016/j.rse.2024.114321, 2024.

1022 Sillman, S.: The relation between ozone, NOx and hydrocarbons in urban and polluted rural

1023 environments, Atmospheric Environment, 33, 1821–1845, https://doi.org/10.1016/S1352-

1024 2310(98)00345-8, 1999.

1025 Steinbacher, M., Zellweger, C., Schwarzenbach, B., Bugmann, S., Buchmann, B., Ordóñez, C.,

1026 Prevot, A. S. H., and Hueglin, C.: Nitrogen oxide measurements at rural sites in Switzerland:

1027 Bias of conventional measurement techniques, J. Geophys. Res., 112, 2006JD007971,

1028 https://doi.org/10.1029/2006JD007971, 2007.

1029 Suleiman, R.: TEMPO gridded NO2 tropospheric and stratospheric columns V03

1030 (PROVISIONAL), https://doi.org/10.5067/IS-40E/TEMPO/NO2_L3.003, 2024.

1031 Thangavel, P., Park, D., and Lee, Y.-C.: Recent Insights into Particulate Matter (PM2.5)-

1032 Mediated Toxicity in Humans: An Overview, IJERPH, 19, 7511,

1033 https://doi.org/10.3390/ijerph19127511, 2022.

1034 Thiagarajan, P. and Ghosh, S.: Jensen–Shannon divergence based novel loss functions for

1035 Bayesian neural networks, Neurocomputing, 618, 129115,

1036 https://doi.org/10.1016/j.neucom.2024.129115, 2024.

1037 Toledo, A. S. O., Silini, R., Carpi, L. C., and Masoller, C.: Outlier mining in high-dimensional

1038 data using the Jensen–Shannon divergence and graph structure analysis, J. Phys. Complex., 3,

1039 045011, https://doi.org/10.1088/2632-072X/aca94a, 2022.

1040 Tsigalou, C., Panopoulou, M., Papadopoulos, C., Karvelas, A., Tsairidis, D., and

1041 Anagnostopoulos, K.: Estimation of low-density lipoprotein cholesterol by machine learning

1042 methods, Clinica Chimica Acta, 517, 108–116, https://doi.org/10.1016/j.cca.2021.02.020, 2021.

1043 Urbanowicz, T., Skotak, K., Filipiak, K. J., Olasińska-Wiśniewska, A., Szczepański, K., Wyrwa,

1044 M., Sikora, J., Tykarski, A., and Jemielity, M.: Long-Term Exposure of Nitrogen Oxides Air

1045 Pollution (NO2) Impact for Coronary Artery Lesion Progression—Pilot Study, JPM, 13, 1376,

1046 https://doi.org/10.3390/jpm13091376, 2023.

1047 2021 TIGER/Line® Shapefiles: https://www.census.gov/cgi-

1048 bin/geo/shapefiles/index.php?year=2021&layergroup=Roads, last access: 21 February 2025.

1049 U.S. 2020 Urban Areas Shapefile:

1050 https://www2.census.gov/geo/tiger/TIGER_RD18/LAYER/UAC20/, last access: 21 February

1051 2025.

1052 Van Der A, R. J., Eskes, H. J., Boersma, K. F., Van Noije, T. P. C., Van Roozendael, M., De

1053 Smedt, I., Peters, D. H. M. U., and Meijer, E. W.: Trends, seasonal variability and dominant NO_x

1054 source derived from a ten year record of NO_2 measured from space, J. Geophys. Res., 113,

1055 2007JD009021, https://doi.org/10.1029/2007JD009021, 2008.

1056 Van Geffen, J., Boersma, K. F., Eskes, H., Sneep, M., Ter Linden, M., Zara, M., and Veefkind, J.

1057 P.: S5P TROPOMI NO₂ slant column retrieval: method, stability,

1058 uncertainties and comparisons with OMI, Atmos. Meas. Tech., 13, 1315–1335,

1059 https://doi.org/10.5194/amt-13-1315-2020, 2020.

1060 Veefkind, J. P., Aben, I., McMullan, K., Förster, H., De Vries, J., Otter, G., Claas, J., Eskes, H. J.,

1061 De Haan, J. F., Kleipool, Q., Van Weele, M., Hasekamp, O., Hoogeveen, R., Landgraf, J., Snel,

R., Tol, P., Ingmann, P., Voors, R., Kruizinga, B., Vink, R., Visser, H., and Levelt, P. F.: TROPOMI on the ESA Sentinel-5 Precursor: A GMES mission for global observations of the atmospheric composition for climate, air quality and ozone layer applications, Remote Sensing of Environment, 120, 70–83, https://doi.org/10.1016/j.rse.2011.09.027, 2012.

Venkatram, A.: Applications of Pollutant Frequency Distributions, Journal of the Air Pollution Control Association, 29, 251–253, https://doi.org/10.1080/00022470.1979.10470788, 1979.

Virta, H., Ialongo, I., Szeląg, M., and Eskes, H.: Estimating surface-level nitrogen dioxide concentrations from Sentinel-5P/TROPOMI observations in Finland, Atmospheric Environment, 312, 119989, https://doi.org/10.1016/j.atmosenv.2023.119989, 2023.

Wang, F. and Zhang, Z.: Correlation Structure and Co-Movement of Hunan Province's Air Pollution: Evidence from the Multiscale Temporal Networks, Atmosphere, 14, 55, https://doi.org/10.3390/atmos14010055, 2022.

Wang, Y., Bechle, M. J., Kim, S.-Y., Adams, P. J., Pandis, S. N., Pope, C. A., Robinson, A. L., Sheppard, L., Szpiro, A. A., and Marshall, J. D.: Spatial decomposition analysis of NO2 and PM2.5 air pollution in the United States, Atmospheric Environment, 241, 117470, https://doi.org/10.1016/j.atmosenv.2020.117470, 2020.

Xia, X., Meng, X., Liu, C., Guo, Y., Li, X., Niu, Y., Lam, K. B. H., Wright, N., Kartsonaki, C., Chen, Y., Yang, L., Du, H., Yu, C., Sun, D., Lv, J., Chen, J., Yang, X., Gao, R., Wu, S., Kan, H., Chan, K. H., Li, L., Chen, Z., Chen, J., Chen, Z., Clarke, R., Collins, R., Li, L., Lv, J., Peto, R., Walters, R., EdrisMohamed, A., Pozarickij, A., Iona, A., Wang, B., Clarke, C., Kartsonaki, C., Schmidt, D., Avery, D., Bennett, D., Fry, H., Du, H., Lam, H., Turnbull, I., Millwood, I., Liu, J., Clarke, J., Chan, K. H., Kolhe, K., Lin, K., Wang, L., Yang, L., Kakkoura, M., Rahmati, M., Barnard, M., Mazidi, M., Wright, N., Yao, P., Ryder, P., Im, P. K., Harish, P., Nie, Q., Stevens, R., Clarke, R., Walters, R., Boxall, R., Morris, S., Gilbert, S., Yang, X., Chen, Y., Chen, Z., Han, X., Hou, C., Xia, Q., Liu, C., Lv, J., Pei, P., Sun, D., Yu, C., Pan, L., Pang, Z., Gao, R., Li, S., Duan, H., Wang, S., Liu, Y., Du, R., Zang, Y., Cheng, L., Tian, X., Zhang, H., Zhai, Y., Ning, F., Sun, X., Li, F., Lv, S., Wang, J., Hou, W., Sun, W., et al.: Associations of long-term nitrogen dioxide exposure with a wide spectrum of diseases: a prospective cohort study of 0·5 million Chinese

adults, The Lancet Public Health, 9, e1047–e1058, https://doi.org/10.1016/S2468-2667(24)00264-0, 2024.

Xu, A. and Xiang, C.: Assessment of the Emission Characteristics of Major States in the United States using Satellite Observations of CO_2, CO, and NO_2, Atmosphere, 15, 11, https://doi.org/10.3390/atmos15010011, 2023.

Yan, J., Li, P., Gao, R., Li, Y., and Chen, L.: Identifying Critical States of Complex Diseases by Single-Sample Jensen-Shannon Divergence, Front. Oncol., 11, 684781, https://doi.org/10.3389/fonc.2021.684781, 2021.

Yu, Z. and Li, X.: The Temporal–Spatial Characteristics of Column NO_2 Concentration and Influence Factors in Xinjiang of Northwestern Arid Region in China, Atmosphere, 13, 1533, https://doi.org/10.3390/atmos13101533, 2022.

Zhang, R., Wang, Y., Smeltzer, C., Qu, H., Koshak, W., and Boersma, K. F.: Reconciling the differences between OMI-based and EPA AQS in situ NO₂ trends, https://doi.org/10.5194/amt-2017-410, 25 January 2018.

Zhao, D., Yan, W., You, M., Zhang, J., Arun, P. V., Jiao, C., Wang, Q., and Zhou, H.: Hyperspectral Anomaly Detection Based on Empirical Mode Decomposition and Local Weighted Contrast, IEEE Sensors J., 24, 33847–33861, https://doi.org/10.1109/JSEN.2024.3455258, 2024.

Zoogman, P., Liu, X., Suleiman, R. M., Pennington, W. F., Flittner, D. E., Al-Saadi, J. A., Hilton, B. B., Nicks, D. K., Newchurch, M. J., Carr, J. L., Janz, S. J., Andraschko, M. R., Arola, A., Baker, B. D., Canova, B. P., Chan Miller, C., Cohen, R. C., Davis, J. E., Dussault, M. E., Edwards, D. P., Fishman, J., Ghulam, A., González Abad, G., Grutter, M., Herman, J. R., Houck, J., Jacob, D. J., Joiner, J., Kerridge, B. J., Kim, J., Krotkov, N. A., Lamsal, L., Li, C., Lindfors, A., Martin, R. V., McElroy, C. T., McLinden, C., Natraj, V., Neil, D. O., Nowlan, C. R., O'Sullivan, E. J., Palmer, P. I., Pierce, R. B., Pippin, M. R., Saiz-Lopez, A., Spurr, R. J. D., Szykman, J. J., Torres, O., Veefkind, J. P., Veihelmann, B., Wang, H., Wang, J., and Chance, K.: Tropospheric emissions: Monitoring of pollution (TEMPO), Journal of Quantitative Spectroscopy and Radiative Transfer, 186, 17–39, https://doi.org/10.1016/j.jqsrt.2016.05.008, 2017.